Seismic Behavior of Unreinforced Masonry Walls with Soft-Layer Strip Bearings

Technical Report

Master Thesis SS 2013

Student: Mr. Arno Barandun
ETHZ
Supervisors: Prof. Dr. Božidar Stojadinović & Dr. Nebojša Mojsilović
ETHZ
Assistant: Dr. Catherine Whyte
ETHZ

Institut für Baustatik und Konstruktion

Eidgenössische Technische Hochschule Zürich

Zürich

01.07.2013

Abstract

Tests on unreinforced masonry wallets with built-in soft-layer membranes were conducted at the ETH Zurich. In practice the soft-layers are positioned at the base of the walls for preventing the propagation of the acoustic noise, the propagation of vibrations, and the capillary rising moisture in the wall.

The aim of the tests was to investigate the behaviour of the wallets with the soft-layers due to horizontal in-plane loading. Initially the wallets were loaded with a vertical load equal to 10 % of their axial strength. After this, a horizontal quasi-static cyclic displacement history was applied at the top of the specimens. The test series included seven different tests. The masonry specimens were built with ordinary Swiss clay bricks (SwissModule B15/19). The dimensions of the wallets were 1.2 m wide (four bricks) and 1.2 m tall (six bricks). Two different soft-layer materials were used for the test: an extruded elastomer material and a rubber granulate material. For each soft-layer material, three different thicknesses (3, 5 and 10 mm) were positioned in the joint above the lowest brick course of the specimens. In addition, a specimen without a soft-layer membrane (control specimen) was tested.

The test series showed promising results. While the specimens with built-in rubber granulate experienced a predominant sliding behaviour along the joint containing the membrane, the control specimen and the specimen with built-in extruded elastomer membrane underwent rocking. The specimens with the rubber granulate dissipated much more energy compared to the control specimen, and the thinner membranes dissipated more energy than the thicker membranes. The material performance of the extruded elastomer is more difficult to quantify because the rocking response of the specimens is mainly caused by their geometry. The results from these tests are very promising for using soft-layer membranes to assist with collapse prevention of masonry walls in an earthquake event.

Furthermore, a finite element model was developed in OpenSees to simulate the behaviour of the specimens. The core element of the model was the BeamColumnJoint (BCJ) element from the OpenSees's element library. The shear panel of the BCJ element was designated to represent the masonry part of the specimen above the joint containing the soft-layer membranes. The three springs at the bottom (two flexure springs and a shear spring) of the BCJ element were simulating the soft-layer membrane. An elastic-no tension (ENT) material was assigned to the flexure springs, and a pinching4 material was assigned to the shear spring. With the ENT material, the model could rock.

The model was very sensitive to the choice of its parameters. Hence only small adjustments were possible without encountering a convergence failure. Therefore the model was adapted. A rigid elastic material was allocated to the flexure spring, and the shear spring material was calibrated to match of the behaviour of the specimen during the experimental tests. For the specimens that experienced a rocking behaviour, a parallel material (combination of a self-centering material and a hysteretic material) was used. To simulate the sliding behaviour, a pinching4 material was assigned to the shear spring. With these adaptions the model was no longer physically correct, but the output of the simulation with the model containing the BCJ element fit the results of the experimental data.

Table of content

List of Figures

List of Tables

Acknowledgements

Acknowledgement

This master thesis could not have been conducted without the help of many different people.

I would like to thank Dominik Werne, Thomas Jaggi, Patrick Morf and Christoph Gisler of IBK's HIF team who helped me during the experimental part of my thesis whenever I needed an extra hand. I could not have carried out the experimental tests without them. Further, I am very thankful to Curdin Bächler and Christian Vögeli who helped me with the preparations and with the conduction of the tests in the laboratory.

Special thanks also go to Kirill Feldman of the Polymer Technologies Group in the Department of Materials at ETH Zurich for conducting the DMA with soft-layer materials.

I am also very grateful to Dr. Catherine Whyte. Her assistance in data processing and development as well as her help for writing the technical report was extremely helpful. I am sure that some errors would have remained undetected without her help. I am very thankful for her support throughout the thesis and especially when I had any problems and also for proof-reading my thesis.

Many thanks also go to Prof. Dr. Stojadinovic and Dr. Mojsilovic who gave me the opportunity to write this master thesis. I gained new and additional knowledge in the use of Matlab and OpenSees, which was a very interesting part of my thesis. I will also keep the experimental part in good memory, even though sometimes the work almost drove me crazy. I am very grateful for the support during this thesis.

Finally I want to thank the people around me. Thanks go to my colleagues who helped me with inputs whenever they were needed and by this made the past years at ETH Zurich a lot easier and more enjoyable.

Very special thanks go to my family, especially to my parents who made these years of interesting study possible.

Thank you all!

1. Introduction

A soft-layer membrane is often placed between the concrete slab and the first course of bricks in typical Swiss unreinforced masonry structural and non-structural walls. The reason for the integration of these polymer based-materials (soft-layers) is mainly to minimize the propagation of the acoustic noise. Furthermore, their use minimizes the propagation of vibrations and protects from capillary rising moisture in the wall. Only soft-layer membranes with a sufficient vertical load capacity are used.

In the past, the vertical load resistance of the soft-layers was investigated. Since the properties of the soft-layer are satisfying and known for this load case, the point of interest is the behaviour in response to horizontal in-plane loads. Information about the mechanical properties of the soft-layer membranes beside the vertical load strength is not known.

Tests with masonry containing soft-layer membranes conducted in the past are summarized below. Griffith & Page (1998) tested small masonry elements composed of three bricks stacked vertically with different types of membranes. The specimens, built with ordinary clay bricks, contained a membrane in each joint. For some tests, the middle brick was replaced with a concrete brick. For these experiments, a monotonic, static cyclic, and dynamic shear force were applied. The ability to transfer shear across the membranes was observed. Furthermore, Zhuge & Mills (1998) and Simundic et al. (2000) reported similar results. Static-cyclic tests with masonry specimens with built-in membranes were performed in the work of Mojsilović et al. (2010). The soft-layers, embossed polythene membranes, were either placed in a mortar joint or a masonry-concrete slab interface. The tests showed a good behaviour subjected to cyclic shear loading. Recently, Mojsilović (2012) conducted experimental tests on masonry specimens (three bricks stacked vertically) with built-in membranes in the bed joint. Three different soft-layer materials (elastomer-, bitumen- and polythene-based) were tested. The shear behaviour of the pre-compressed specimen was observed. The performance showed considerable energy dissipation and also large deformation capacity (Mojsilović, 2012).

Ten experimental tests were conducted in this study to better understand the behaviour of specimens containing soft-layer membranes. Two different membranes were investigated: an extruded elastomer material and a rubber granulate material. Each material was tested with three different thicknesses (3, 5 and 10 mm). Additionally, a wallet without a soft-layer membrane was tested. The specimens were four bricks wide (1.2 m) and six bricks tall (1.2 m).

The specimens were first loaded with a vertical load up to 10 % of their vertical load strength. After the vertical load was applied, a horizontal quasi-static displacement sequence was applied at the top of the wallets.

During the Fall semester 2012, seven specimens were tested in a master project thesis. In continuation of this work in the Spring semester 2013, three specimens had to be repeated. The conduct of these three experimental tests and the processed data obtained from the ten experimental tests are incorporated in the current master thesis. The horizontal force displacement diagram (hysteresis), the response envelope (backbone curve), the damage, and the dissipated energy of each of the specimen were compared.

Considering the results of the experimental tests, a finite element model for numerical simulation was developed. The model was compiled using OpenSees. The core element of the model was the BeamColumnJoint (BCJ) element from the OpenSees's element library. The shear panel of the BeamColumnJoint element was designated to represent the masonry part of the specimen above the joint containing the soft-layer membranes. The three springs at the bottom of the BeamColumnJoint element were simulating the soft-layer membrane. The model was calibrated to the experimental test results by adjusting the properties of its components.

2. Experimental Part

2.1. The Building Materials

2.1.1. Bricks

The wallets were built with clay bricks. All bricks originate from the same batch at a brick factory. They were of the type of SwissModul B15/19 (Figure 1). According to the Swisscode (SIA) 266 Masonry the minimum required vertical load strength is 7 N/mm.

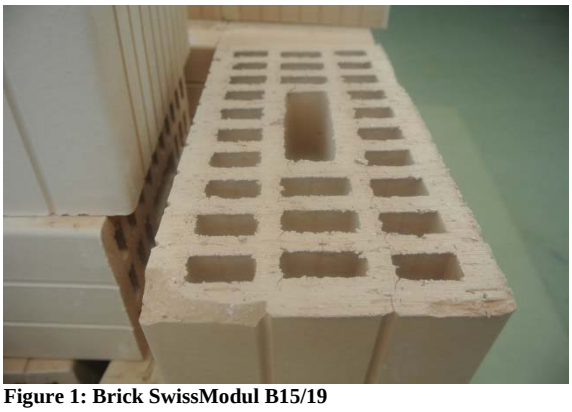

Figure 1: Brick SwissModul B15/19

The testing and research institute “p+f sursee” conducted the material tests of the bricks. The results are summarized in the following table.

Type of Brick	SwissModule B15/19
Length [mm]	289
Height [mm]	148
Width [mm]	190
Pressure Strength [MPa]	25.5
Standardized Pressure Strength [MPa]	30.8
Cross Tension Strength [MPa]	7.2
Form Factor [-]	1.21
Void Area [%]	43
Mass of a Brick [g]	7591
Bulk Density [kg/m^3]	935
Moisture Suction [kg/(m^2 min)]	2.8

Table 1: Test Results of the Bricks SwissModul B15/19

2.1.2. Mortar

For building the specimens, ordinary cement mortar was used. The masons built the specimens in two work sessions. Each time six prism samples of the mortar were taken for evaluation of the mechanical properties. Three of the six samples stayed in the laboratory for hardening next to the masonry specimens; the other three were stored in an air-conditioned room with an increased humidity. The dimensions the prism samples were 40/40/100 mm. The Table 2 shows the results of the mortar tests.

Sample	Description	Bending		Pressure			
		[kN]	[MPa]	[kN]	[kN]	[MPa]	[MPa]
H1	Built: 19.10.12, dried in the labratory	2.5	5.7	35.7	36.8	22.3	23
H2	Built: 19.10.12, dried in the labratory	2.2	5.1	31.6	34	19.8	21.3
H3	Built: 19.10.12, dried in the labratory	2	4.5	33.6	36	21	22.5
	Mean value	2.23	5.10	34.62		21.65	
	Standard deviation	0.25	0.60	1.92		1.18	
F1	Built: 19.10.12, dried in the air-conditioned room	2	4.6	34.3	33.6	21.4	21
F2	Built: 19.10.12, dried in the air-conditioned room	2.2	5.3	35.8	36.2	22.4	22.6
F3	Built: 19.10.12, dried in the air-conditioned room	2.2	5	33.5	37.8	20.9	23.6
	Mean value	2.13	4.97	35.20		21.98	
	Standard deviation	0.12	0.35	1.70		1.06	
H1R	Built: 25.02.13, dried in the labratory	1.3	3.1	13.8	11.9	8.6	7.5
H2R	Built: 25.02.13, dried in the labratory	1.4	3.2	18.1	13.5	11.3	8.4
H3R	Built: 25.02.13, dried in the labratory	1.2	2.8	12.8	11.8	8	7.4
	Mean value	1.30	3.03	13.65		8.53	
	Standard deviation	0.10	0.21	2.33		1.44	
F1R	Built: 25.02.13, dried in the air-conditioned room	1.7	4	16.3	16.9	10.2	10.6
F2R	Built: 25.02.13, dried in the air-conditioned room	1.6	3.7	18	18.1	11.3	11.3
F3R	Built: 25.02.13, dried in the air-conditioned room	1.7	3.9	16.6	19.1	10.3	11.9
	Mean value	1.67	3.87	17.50		10.93	
	Standard deviation	0.06	0.15	1.08		0.67	

Table 2: Results of the Mortar Tests

2.1.3. Soft-Layers

Two different materials were explored as soft-layer membranes integrated in the masonry specimens: an extruded elastomer material (E) and a rubber granulate material (G). Each of these soft-layer membranes were tested with three different thicknesses, namely 3, 5 and 10 mm.

Figure 2: Extruded Elastomer (E)

Figure 3: Rubber Granulate (G)

Very little information exists about the mechanical properties of the soft-layers. The supplier only provides that a minimum vertical load strength (5 MPa) (Mageba, 2013) is achieved. More information is available on acoustic and insulating properties.

The Polymer Technologies Group of the Department of Materials of the ETH Zurich has conducted a dynamic material analysis (DMA) of the two polymers. In a DMA (Menczel & Prime), a sinusoidal load pattern is applied to viscoelastic materials, normally polymers. Usually a phase lag is visible in the time histories of the force and the deformation.

In addition to the amplitude of the force and the amplitude of the deformation, the phase lag is the basis for the calculation of the elasticity modulus E*. This parameter has two parts: the storage modulus E’ and the loss modulus E’’. The storage modulus, the real part, is representing stored mechanical energy in the system. The loss modulus, the imaginary part, shows how much energy has been dissipated by the material. By using the formula of Pythagoras the modulus of elasticity E* can be calculated. In this case the Polymer Technologies Group measured the shear modulus G.

The DMA can be conducted by varying different parameters. In this case, the researcher of the Polymer Technologies Group of the ETH Zurich did the DMA by varying the temperature. The diagram 4 show the shear modulus G for extruded elastomer material and the granulate rubber material.

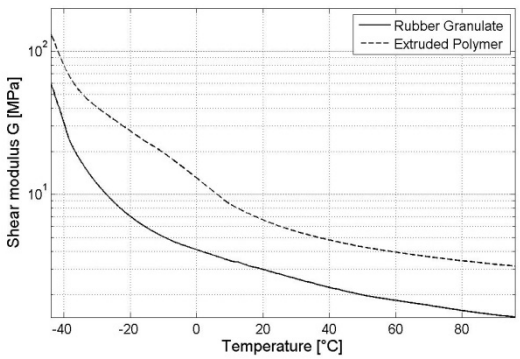

Figure 4: Shear Modulus of the Soft-Layer over the Temperature

2.1.4. Specimen

The dimensions of the masonry specimens were 1.2 m x 1.2 m. All the clay brick wallets included a polymer membrane (soft-layer) joint above the bottom row of bricks. This polymer was laid directly on the bricks. The masons put a layer of mortar on this membrane and continued above with the wallet in an ordinary manner. To ensure the quality of the masonry, two professional masons were hired to build the walls.

Initially seven specimens were built: three for each soft-layer material plus one for the control specimen (without soft-layer). The different thicknesses of the polymer membranes were 3 mm, 5 mm and 10 mm. For the walls with 3 mm and 5 mm membranes, the thickness of the mortar layer in this joint was chosen to be 7 mm and 5 mm, respectively. The result was the same 10 mm overall joint thickness for these specimens. For the walls with 10 mm thick soft-layers, the mortar layer thickness was 5 mm.

Figure 5: 10 mm Joint (WG5 pictured)

Figure 6: 15 mm Joint (WE10 pictured)

Due to problems with the test setup, the first three tests had to be repeated. Table 3 shows an overview of the labelling of the different specimens. The capital letter R signals a repetition test.

Label	Material	Layer Thickness	Joint Thickness [mm]
W0	-	-	10
W0R	-	-	10
WG3	Rubber	3	10
WG5	Rubber	5	10
WG10	Rubber	10	15
WE3	Extruded	3	10
WE5	Extruded	5	10
WE10	Extruded	10	15
WE3R	Extruded	3	10
WE5R	Extruded	5	10

Table 3: Labelling of the Specimen

The wallets were built in running bond with four bricks per layer and six in height. Every specimen had to harden 28 days before testing. In Figure 7 a picture and in Figure 8 a drawing of a specimen is shown.

Figure 7: Picture of a Specimen

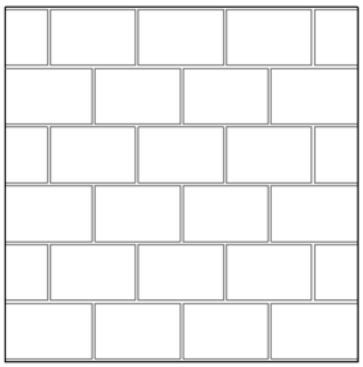

Figure 8: Drawing of a Specimen

For a better investigation of the development of the cracks, the wallets were painted white on one side.

2.2. Test Procedure

All specimens were tested in the HIF laboratory of the ETH Zurich.

2.2.1. Test Setup

The test setup is shown in Figure 9 and Figure 10. The vertical load was applied by hydraulic jacks (2) located between a support beam (1) and the upper spreader beam (3). For decoupling the upper spreader beam horizontally from lower spreader beam (4) a roller bearing was arranged. The specimen was laid on a baseplate (7) in a mortar bed. The baseplate was fixed to the strong floor (8) of the laboratory. A mortar layer (9) was placed between the specimen and the lower spreader beam. To prevent sliding along the joint between the baseplate and the first course of bricks stoppers (10) were installed.

For applying the horizontal force, a hydraulic actuator (12) was used. The actuator pushed and pulled the lower spreader beam. To generate the force a reaction wall (13) was needed.

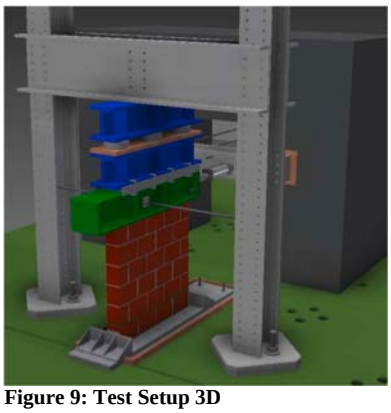

Figure 9: Test Setup 3D

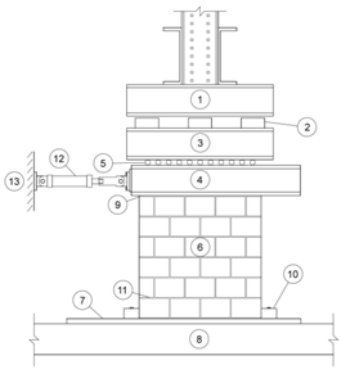

Figure 10: Test Setup 2D

2.2.2. Measurement Setup

16 sensors were installed for measuring the deformation. Furthermore the vertical pressure and the horizontal force were recorded. At the horizontal jack a Potentiometer was positioned, which was controlling the applying displacement according to the defined displacement pattern. The layout of the potentiometers can be seen in Figure 11.

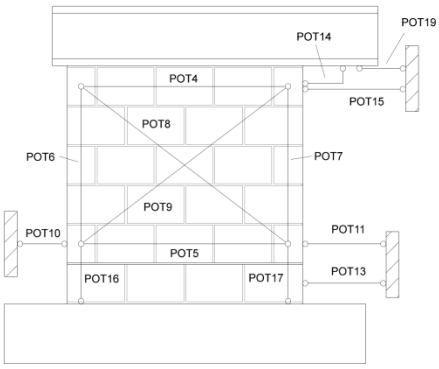

Figure 11: Measurement Setup

Two potentiometers recorded the vertical deformations (POT6 and POT7) in the wall, two recorded the horizontal deformations (POT4 and POT5), and two recorded the diagonal deformations (POT8 and POT9). Another two potentiometers were measuring the uplift (POT16 and POT17) between the

baseplate and the first brick above the soft-layer, so they captured the uplift of the wall on one side and the compression of the soft-layer on the other.

The absolute displacement was measured at the top of the wall: once below the soft-layer (POT13), once directly above the soft-layer (POT11) and once at the top brick of the specimen (POT15). Additionally there were three potentiometers for redundancy (POT10, POT14 and POT15).

2.2.3. Preparations for the Tests

All wallets were built in one corner of the lab, where they could rest until testing. Before testing, they were picked up with a fork lift, laid in a previously prepared mortar bed, and aligned. In the next step mortar was put on the top of the wall to connect to the lower spreader beam.

Afterwards the measurement setup was installed.

2.2.4. Procedure of the Test

After all required components were ready for testing, 10 % of vertical load strength of an ordinary masonry wall was applied. In the following formula $F_{vertical}$ is the vertical applied force, which is computed with the area of the masonry section ($A_{masonry}$), the strength of the masonry ($f_{u,masonry}$) and the mass of the beams above the specimen ($m_{topBeams}$).

$$F_{vertical} = 0.1 \cdot A_{masonry} f_{u,masonry} - m_{topBeams} = 100.9\ kN$$

During the first three tests (which were to be repeated later), the vertical force was not held constant due to rocking of the wall. A pendulum manometer was used for the following tests, which could regulate the vertical load to a constant level.

The horizontal force was applied directly on the beam above the specimen. With this assembly, the horizontal load was applied in a consistent manner. The loading pattern was sinusoidal, and the amplitudes are shown in Table 4.

Target displacement [mm]	Loading speed [mm/min]	Duration [min]
0.2	1	1.6
0.5	1	4.0
1.0	1	8.0
1.5	1	12.0
2.0	3	5.3
5.0	3	13.3
10.0	3	26.7
15.0	10	12.0
20.0	10	16.0
30.0	10	24.0
40.0	20	16.0

Table 4: Loading Pattern

After each loading step the cracks were tagged on the wall and photographed. The interesting damage zones and uplifts were photographed.

2.3. Results of the Tests

The specimens were tested all in the same manner. The first seven tests were conducted in the context of the project thesis in the fall semester 2012, and the repetition test were integrated in the master thesis of the spring semester 2013.

The specimens tested in the fall semester (labelled without R) were initially pulled. Due to the replacement of the controller of the test setup, the repetition experiments (labelled with R) were initially pushed. For the presentation of the results, the initial movement, whether it was push or pull, is considered positive for all specimens.

Due to limitations of the test setup, the jack travel was confined to a cycle with maximum 20 mm amplitude if a rocking behaviour occurred. The space between the vertical presses and the beam above them allowed only a certain amount of tilting. In the case of WE10 the maximum uninfluenced amplitude was 15 mm.

This behaviour leads to an inhibition of cycles larger than 20 mm because the rocking motion at approximately 20 mm leaded to a lack of space of the vertical presses (Figure 12). The specimen could not deform beyond this point.

Figure 12: Picture of the Lack of Space at the Vertical Jack

2.3.1. Control Specimen

The wallet without any soft-layer (W0) was tested to obtain the results of a comparable ordinary masonry wall. The results of the wallets with the soft-layers could be compared with each other and to the ordinary masonry, too. The W0 specimen was the first test of this test series. The results were unusable due to problems with the test setup. Therefore the test had to be repeated (W0R) in the spring semester. In Figure 13 the displacement history and in Figure 14 the vertical load history is shown. The plots have the same time axis, so they can be compared directly to each other. At the end of the test the vertical force dropped immediately. This happened because the experiment was stopped.

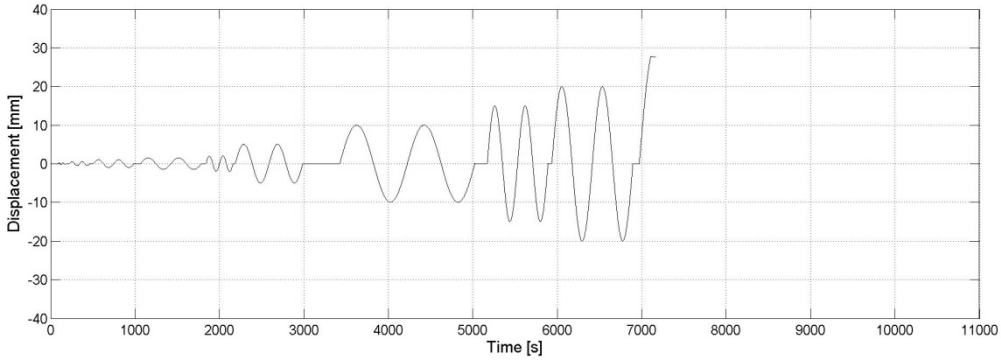

Figure 13: Displacement History W0R

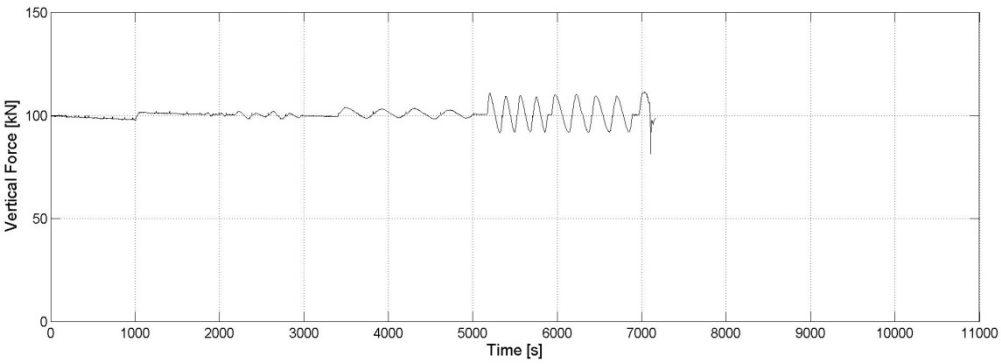

Figure 14: Vertical Load History W0R

Due to the cyclic horizontal loading, the vertical force was difficult to hold constant. After increasing the oil flow to the pendulum manometer, the variations of the force were minimized, but it was not possible to prevent them. The magnitude of the force oscillations were much smaller compared to the tests without pendulum manometer.

The hysteresis (Figure 15) shows the horizontal force plotted against the applied displacement of the horizontal jack. During the test, uplift was observed.

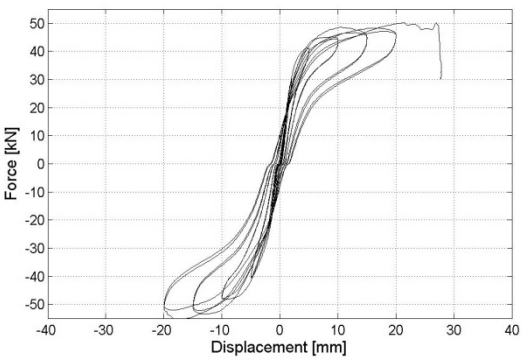

Figure 15: Hysteresis W0R

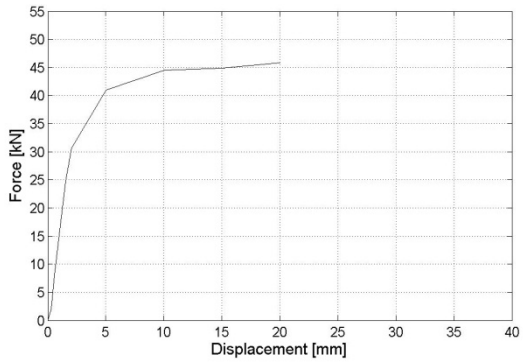

Figure 16: Backbone Curve W0R

The pushover curve (Figure 16) was constructed according to the American Society of Civil Engineers Seismic Rehabilitation of Existing Building Guidelines (ASCE 41-06). The points of peak displacement during the first cycle of each displacement amplitude were connected.

Additionally the damping coefficient for each data set has been computed. It was done according to Dynamic of Structures (Chopra, 2007). The damping ratio shows the development of the dissipated energy per cycle over all cycles. It is calculated (formula below) by the ratio of the dissipated energy per cycle (E_D) divided by the strain energy (E_{So}).

$$\xi = \frac{1}{4\pi}\frac{E_D}{E_{So}}$$

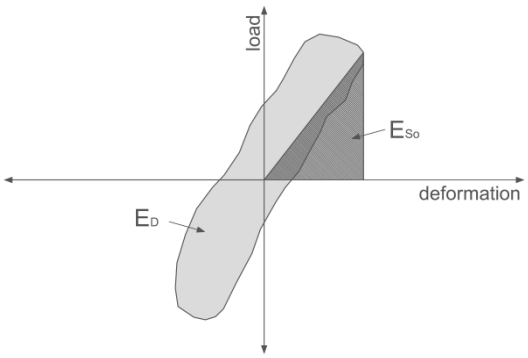

Figure 17: Areas for Computing the Damping Ratio

In Figure 18 the first and the second cycle damping ratios are shown.

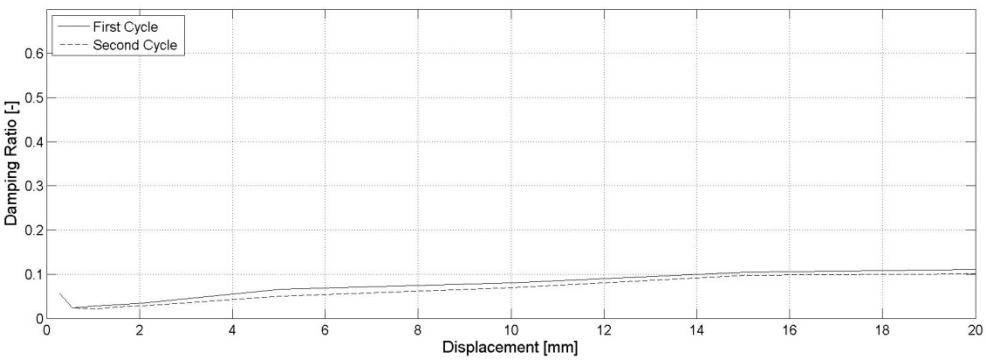

Figure 18: Damping Ratio W0R

2.3.2. Extruded Elastomer (WE)

An overview of the test results can be seen in the following figures. The tests of the WE-series had to be stopped after the cycles with 20 mm amplitude because of the minimal space between the vertical jacks and the upper spreader beam above. These walls exhibited predominately rocking behaviour, which made the problem with the vertical jacks worse. As one side of the wall uplifted, the space between that vertical jack and the beam was further minimized.

The displacement history and the vertical force history of the specimen with the 3 mm thick built-in extruded elastomer soft-layer are shown in Figure 19 and Figure 20, respectively.

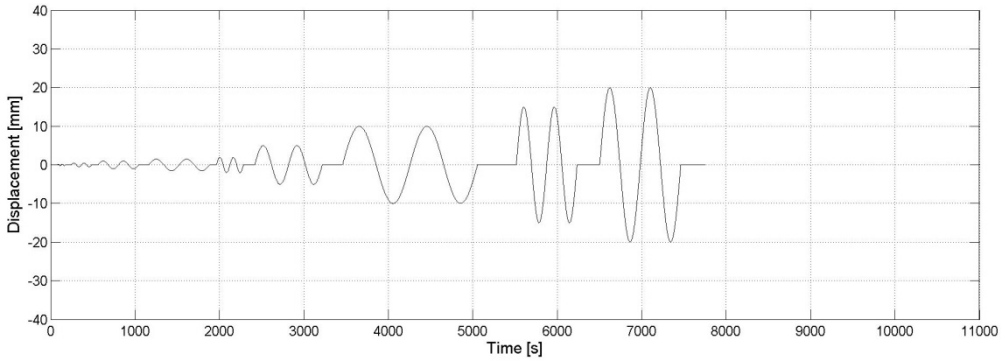

Figure 19: Displacement History WE3R

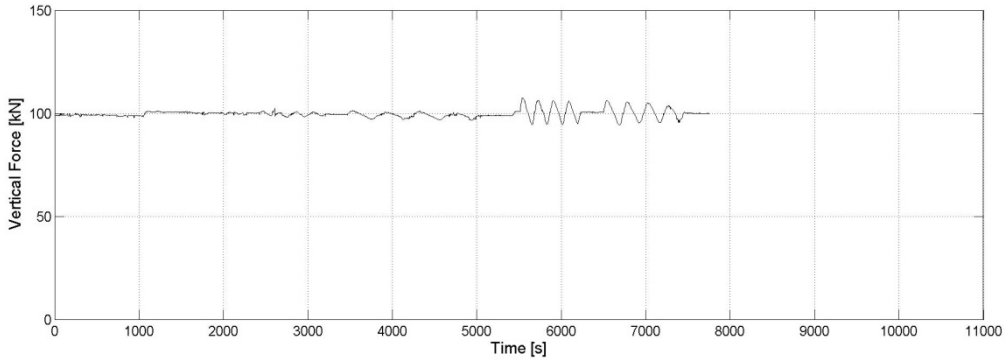

Figure 20: Vertical Load History WE3R

Figure 21 and Figure 22 show the time histories of specimen WE5R

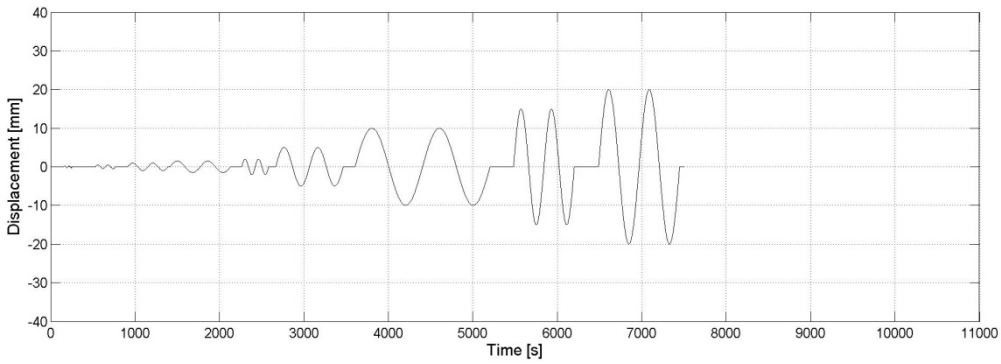

Figure 21: Displacement History WE5R

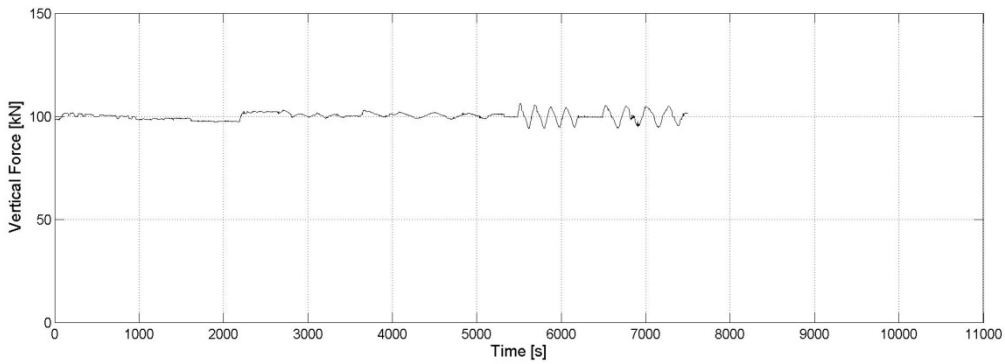

Figure 22: Vertical Load History WE5R

The experimental test of WE10 had to be stopped during the first cycle with 20 mm amplitude (Figure 23), because the vertical jack was contacting the upper spreader beam and was influencing the results. The vertical load history is shown in Figure 24.

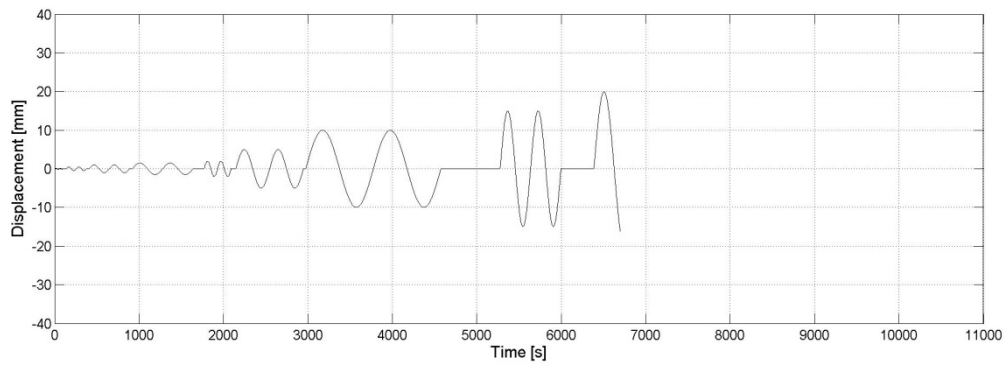

Figure 23: Displacement History WE10

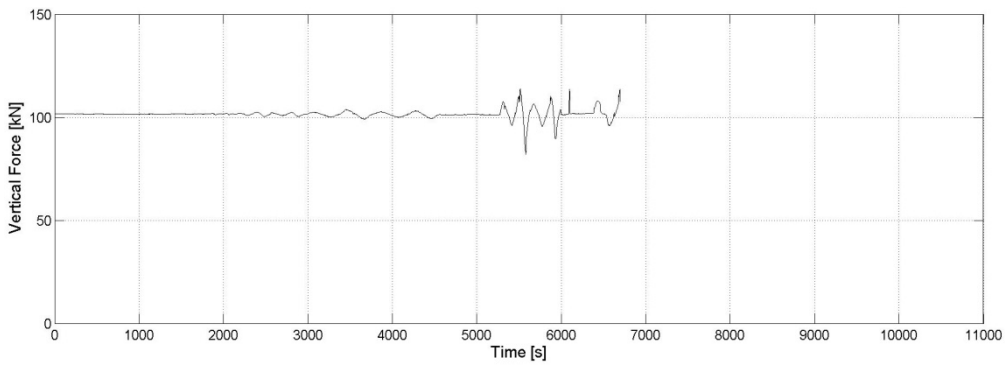

Figure 24: Vertical Load History WE10

The following figures show the hysteresis of the WE-series on the left side and the backbone curve on the right side. For comparison, the backbone curve of the W0R control specimen is additionally plotted.

The hysteresis of the WE3R (Figure 25) looks symmetrical. A degradation of the strength occurred for larger cycles, which is apparent in the backbone curve in Figure 26.

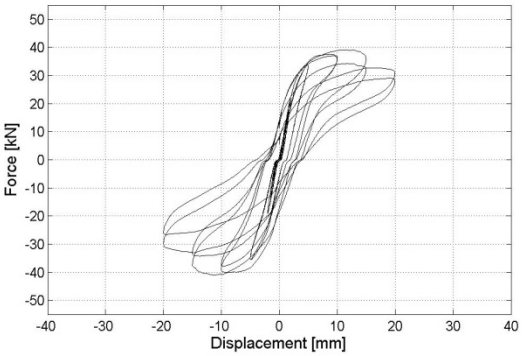

Figure 25: Hysteresis WE3R

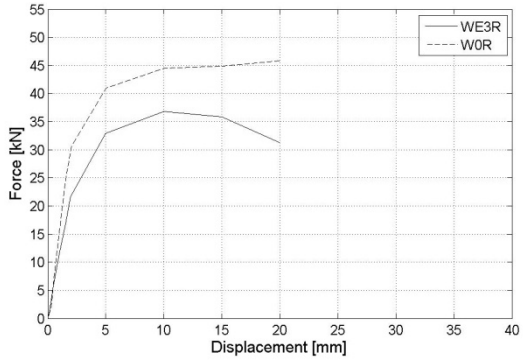

Figure 26: Backbone Curve WE3R

The WE5R specimen displayed similar behaviour. In the hysteresis (Figure 27), hardening can be observed (displacement amplitude 20 mm) on the negative side. This happened because of the limitations of the test setup for rocking behaviour. The backbone curve is shown in Figure 28.

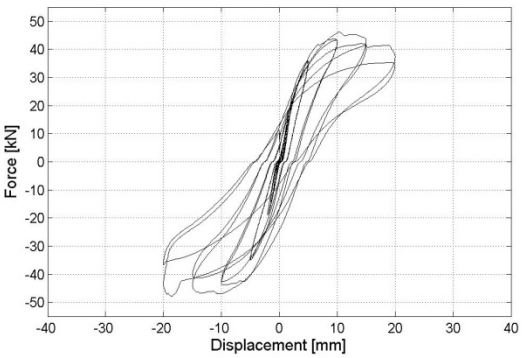

Figure 27: Hysteresis WE5R

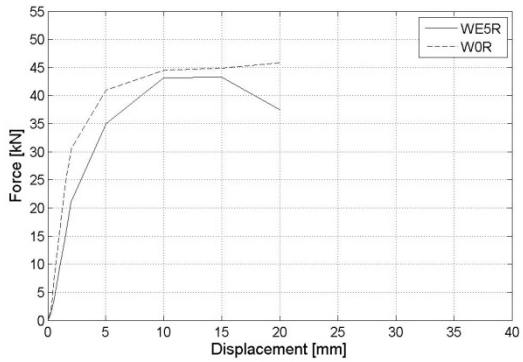

Figure 28: Backbone Curve WE5R

In Figure 29, the hysteresis of the WE10 specimen is shown. For the cycle with 20 mm displacement, hardening occurred. Again, this happened because of the limitations of the test setup for rocking behaviour (Figure 12). In the corresponding backbone curve (Figure 30), this 20 mm cycle is not included. Thus the backbone curve ends at a displacement of 15 mm.

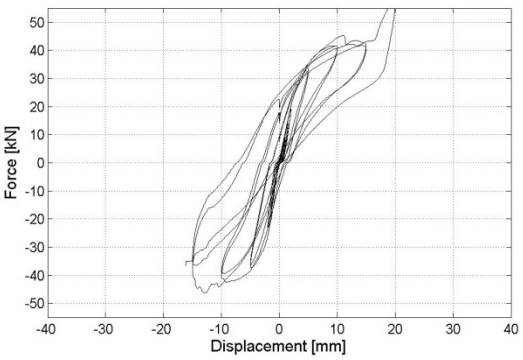

Figure 29: Hysteresis WE10

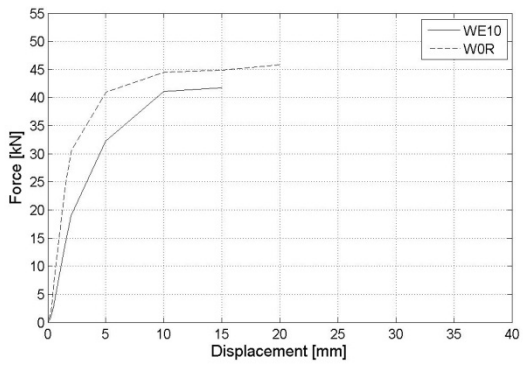

Figure 30: Backbone Curve WE10

In the following graphs, the damping ratios over all cycle amplitudes are shown. In each plot, one graph represents the first cycles of the amplitudes and the other represents the second ones. The energy dissipation of the WE-series was for all specimens higher than the one of the control specimen.

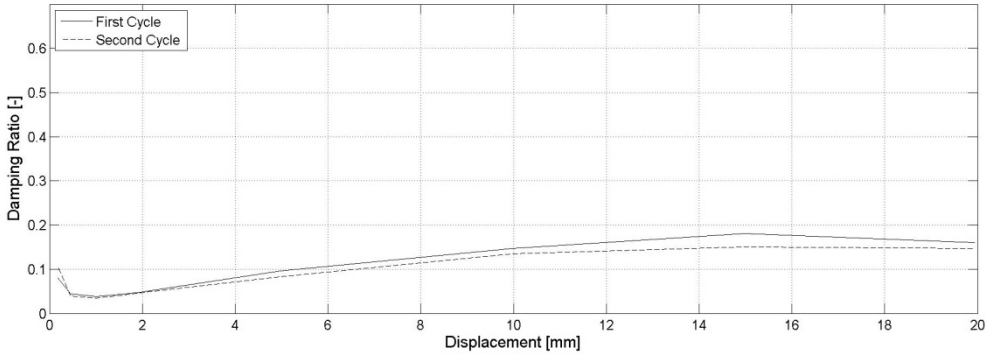

Figure 31: Damping Ratio WE3R

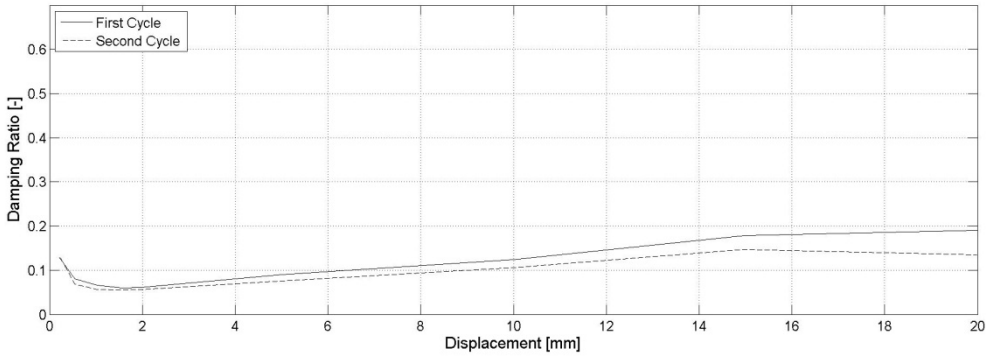

Figure 32: Damping Ratio WE5R

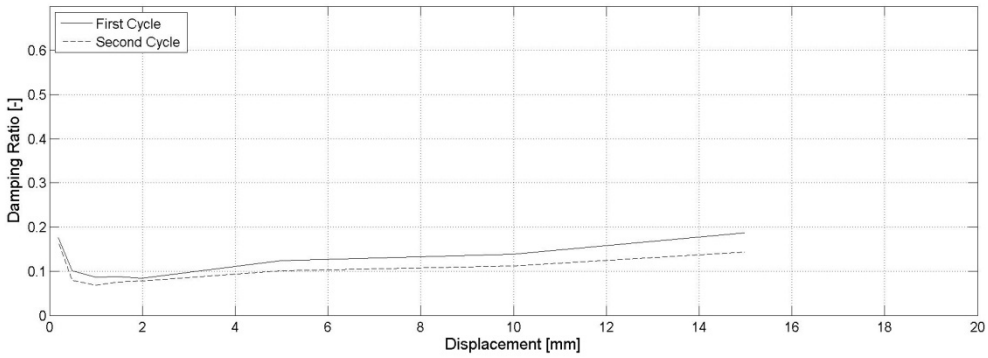

Figure 33: Damping Ratio WE10

After the tests were conducted, the soft-layers were photographed. The pictures give information about the damage which occurred in the membranes during the tests. For the WE-series (Figure 34 – 36), the soft-layers were hardly damaged.

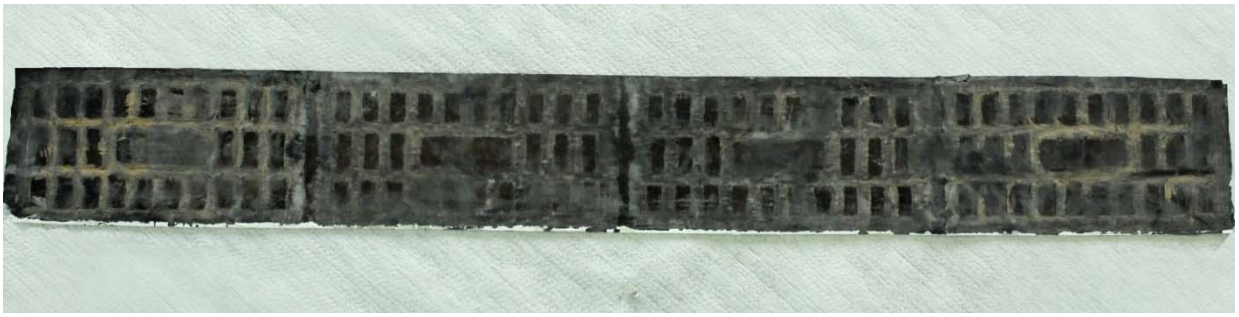

Figure 34: Soft-Layer Damage WE3R

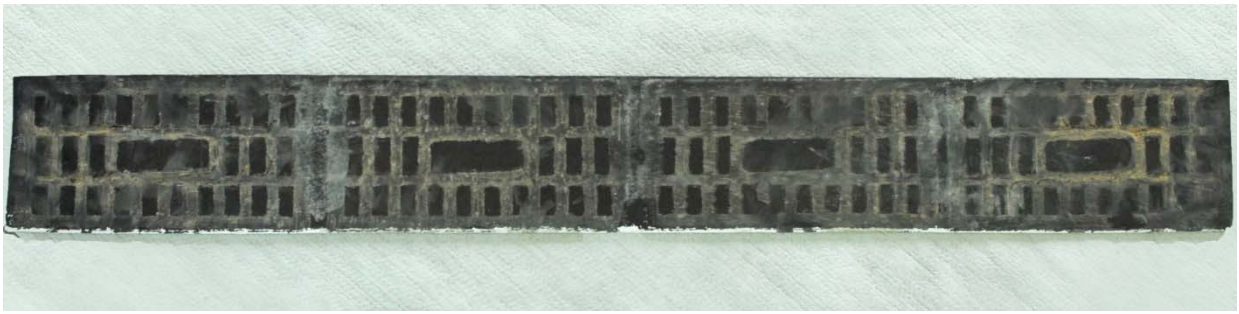

Figure 35: Soft-Layer Damage WE5R

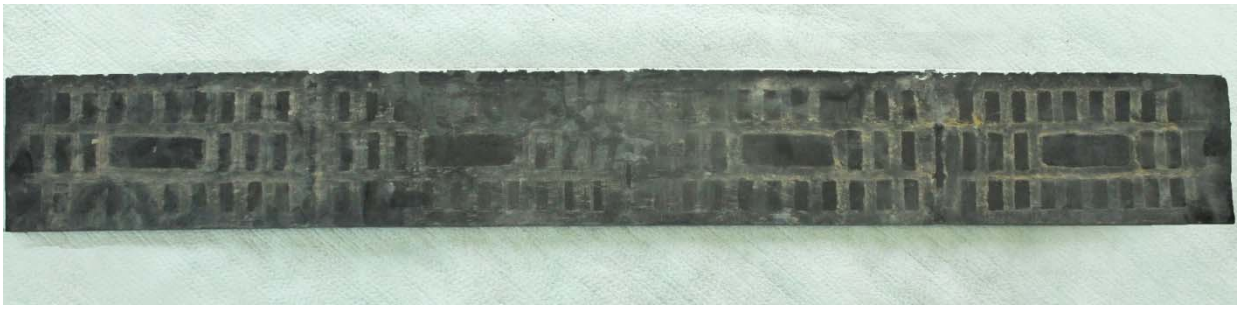

Figure 36: Soft-Layer Damage WE3R

2.3.3. Rubber Granulate (WG)

The wallets containing a soft-layer of rubber granulate experienced predominately sliding behaviour, so a maximum of 30 mm horizontal displacement was achieved before experiencing difficulties with the vertical jacks. The displacement and vertical force histories (figures below) are shown in the same way as for the WE-series.

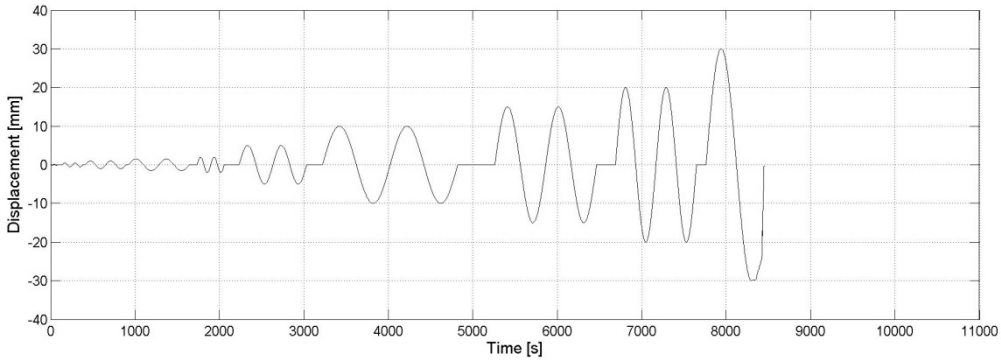

Figure 37: Displacement History WG3

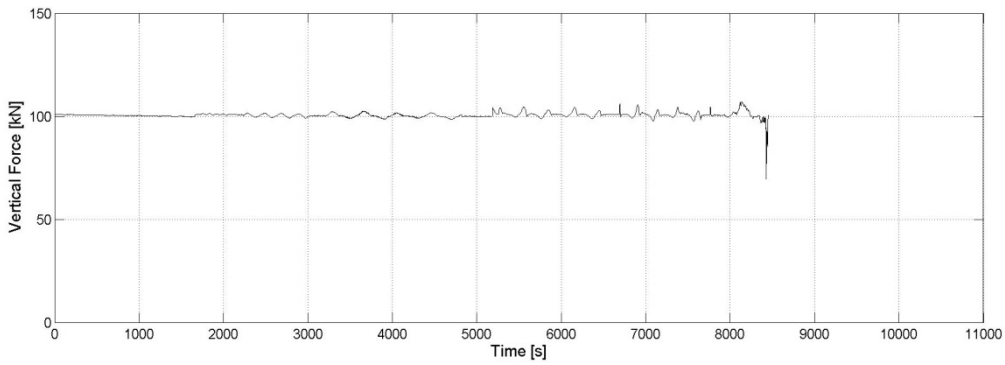

Figure 38: Vertical Load History WG3

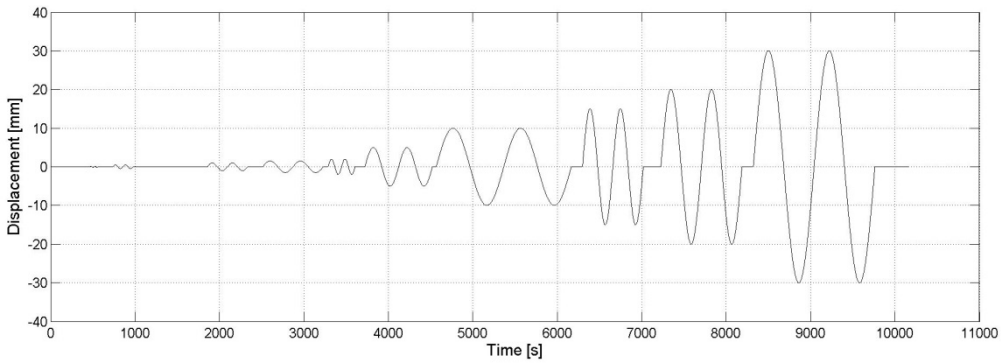

Figure 39:: Displacement History WG5

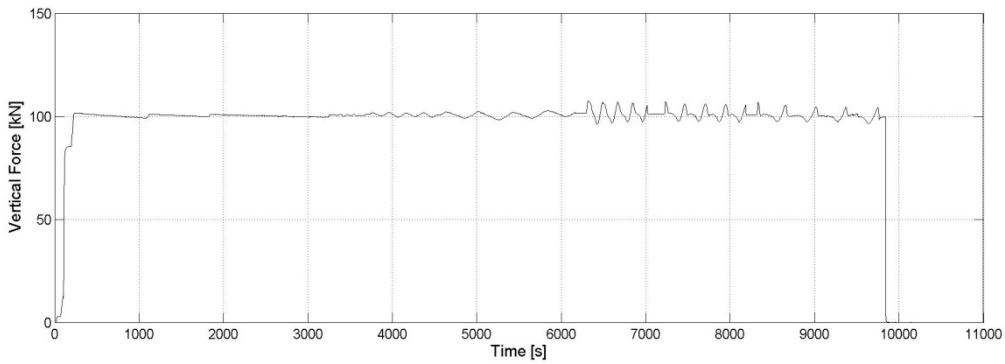

Figure 40: Vertical Load WG5

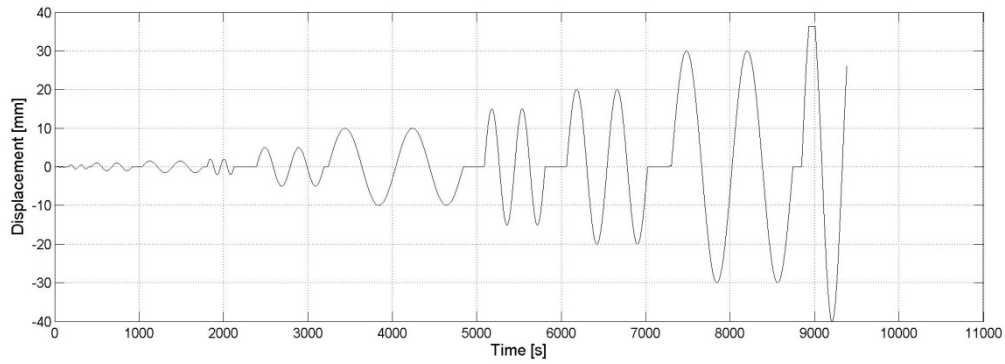

Figure 41: Displacement History WG10

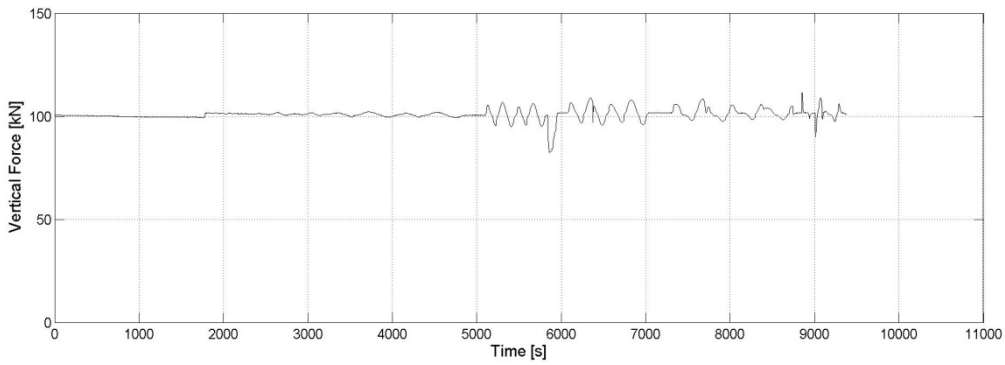

Figure 42: Vertical Load History WG10

The hysteresis and the backbone curves are shown in the following figures. The backbone curve of W0R is integrated in all the backbone curves, like it is in the ones of the WE-series.

The hysteresis plot of WG3 (Figure 43) shows the whole test including the final cycle when the vertical load was released. In the diagram you can see the releasing path after the negative amplitude of the 30 mm cycle. In the backbone curve (Figure 44) you can observe rapid strength degradation.

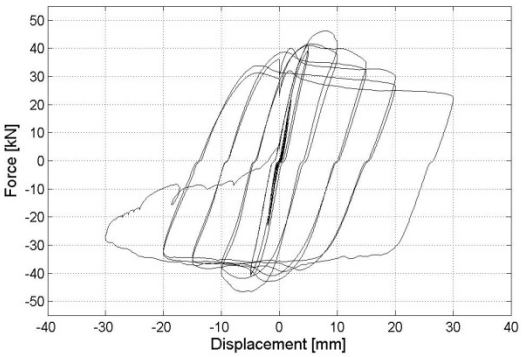

Figure 43: Hysteresis WG3

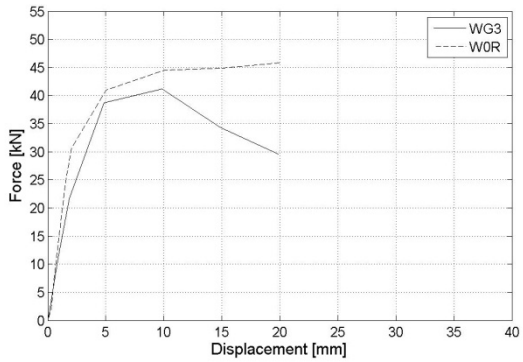

Figure 44: Backbone Curve WG3

The following two figures show the hysteresis (Figure 45) on the left and the backbone (Figure 46) on the right for the WG5 specimen. This specimen also experienced strength degradation with increasing cycle displacement.

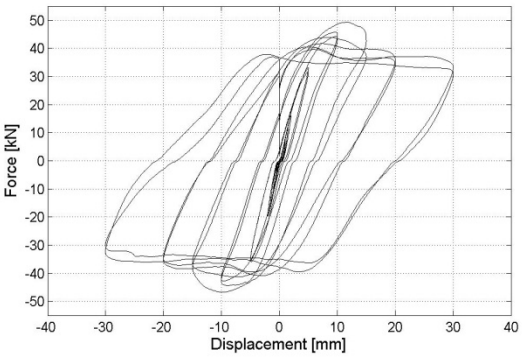

Figure 45: Hysteresis WG5

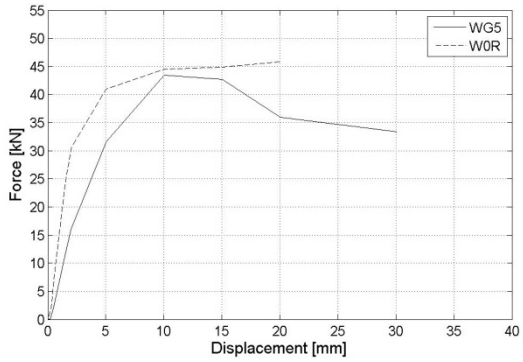

Figure 46: Backbone Curve WG5

The results of specimen WG10 are shown below. The hysteresis is on the left in Figure 47 and the backbone curve on the right in Figure 48. During the cycles with smaller amplitudes, some uplift was observed, but not as much as for the WE-series. Like the other WG-series specimens, this specimen also experienced strength degradation.

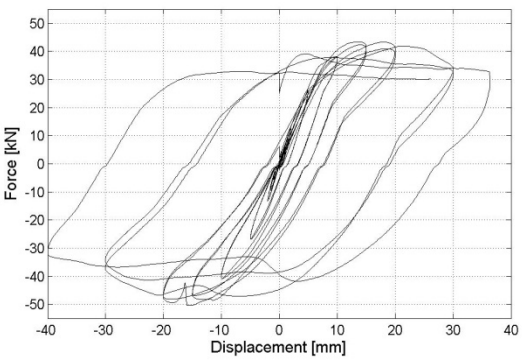

Figure 47: Hysteresis WG10

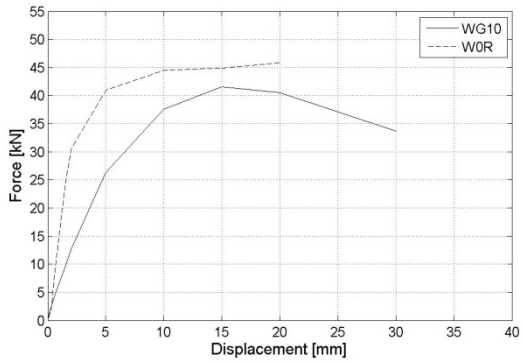

Figure 48: Backbone Curve WG10

The damping ratios for the first and second cycle for each specimen with the built-in rubber granulate membrane are shown in the following three plots. The WG-series showed a bigger energy dissipation compared to the WE-series.

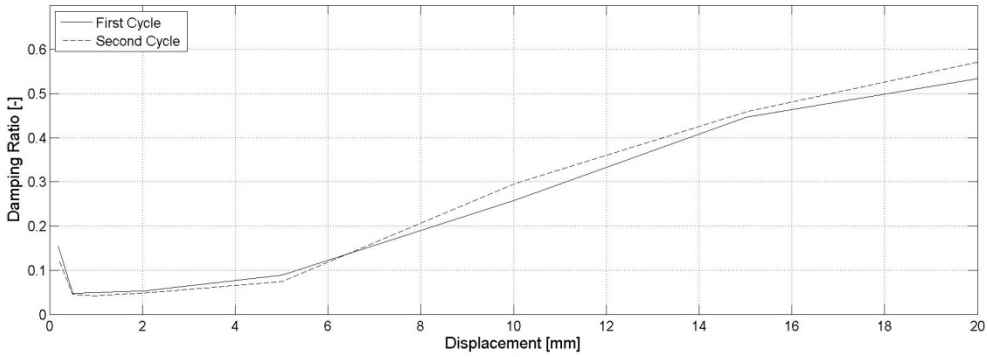

Figure 49: Damping Ratio WG3

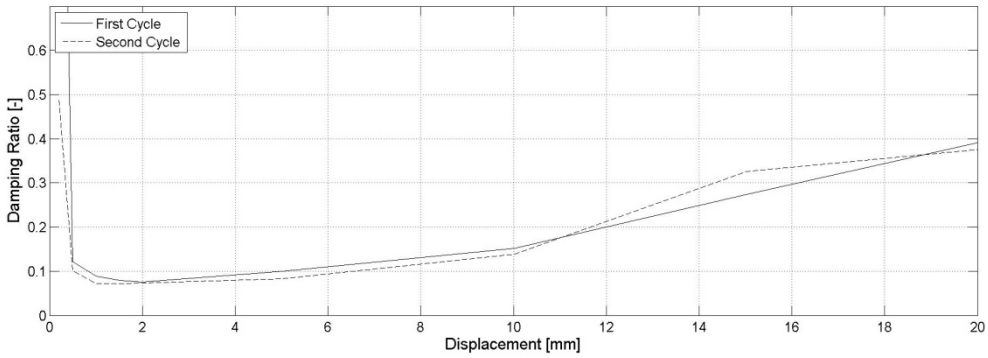

Figure 50: Damping Ratio WG5

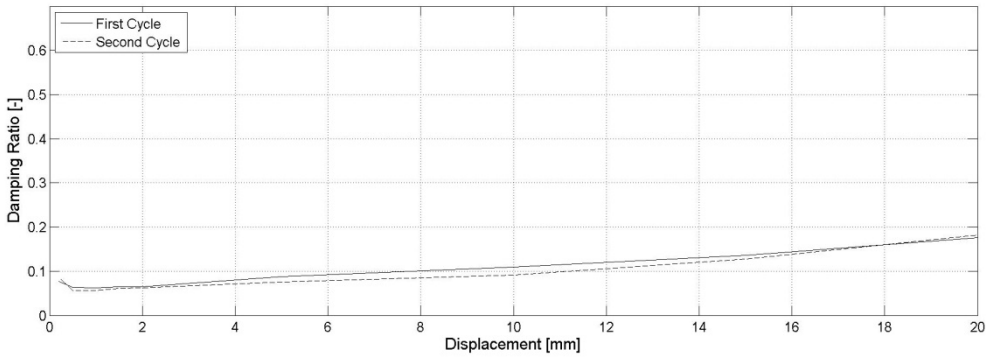

Figure 51: Damping Ratio WG10

The appearances of the soft-layers after the experiments are shown in the following pictures. The rubber granulate soft-layers experienced severe damage.

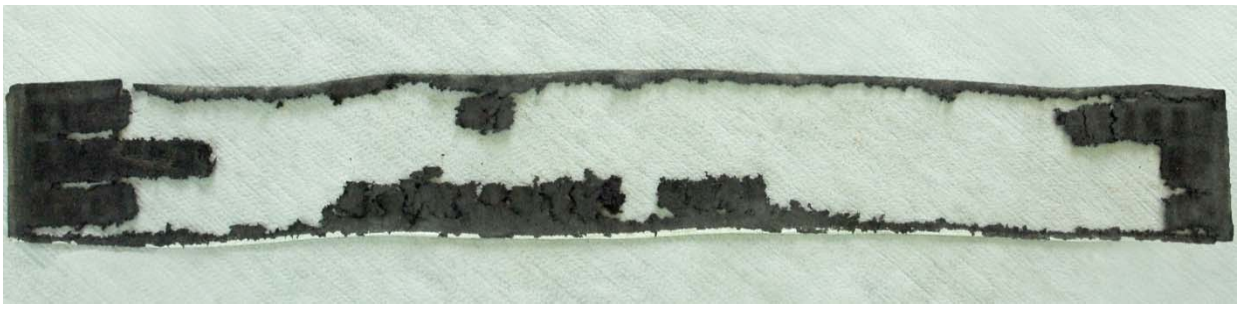

Figure 52: Soft-Layer Damage WG3

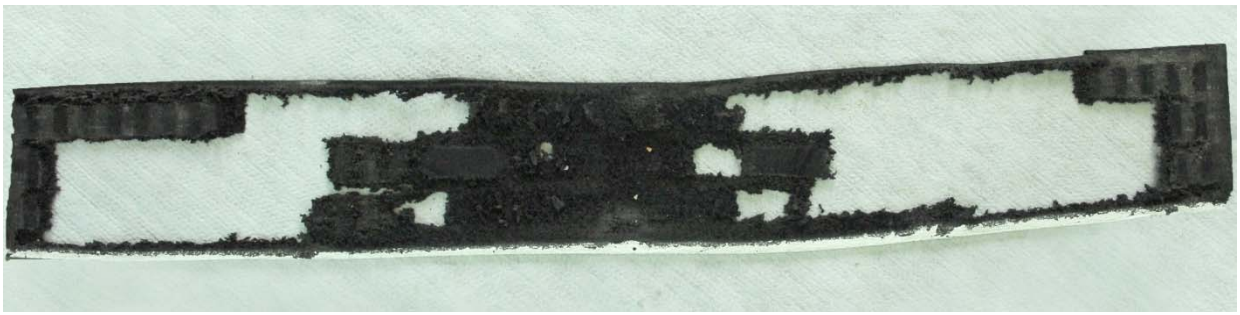

Figure 53: Soft-Layer Damage WG5

Figure 54: Soft-Layer Damage WG10

2.4. Conclusion of the Experimental Part

2.4.1. Cracks

As shown in the figures above, the hysteresis of the WE-series has an s-shaped appearance. The reason for that is a predominant occurrence of rocking. In this case, the masonry part primarily experienced a rigid body motion. However, it also dissipated some energy, observed by the development of the cracks (Figure 55), so the hysteresis does not look like a perfect rocking curve. The corner brick at the bottom failed based on a combined sliding and compression failure (Figure 56).

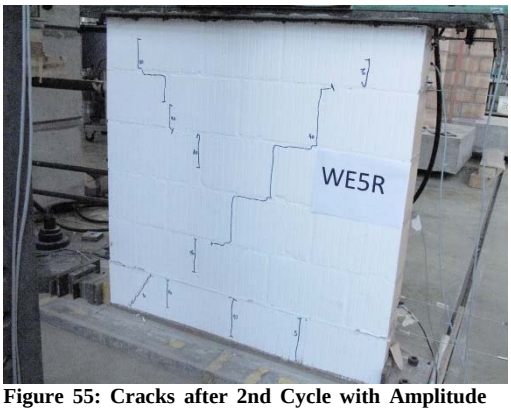

Figure 55: Cracks after 2nd Cycle with Amplitude 10 mm of WE5R

Figure 56: Damaged Bricks after the Test WE10

In case of the control specimen the hysteresis is also s-shaped. The cracks developed in an earlier cycle of the test compared to the specimens with built-in soft-layer. Since very little sliding occurred in this specimen, almost all of the dissipated energy had to be generated by cracking. Figure 57 shows the state of the cracks of the control specimen after the second cycle with amplitude 10 mm (compare with Figure 55 and 59). Furthermore the damaged corner of W0R after the test can be seen in Figure 58.

Figure 57: Cracks after 2nd Cycle with Amplitude 10 mm of W0R

Figure 58: Damaged Lateral Bricks after the Test W0R

The behaviour of WG-series specimens was mainly influenced by sliding. During the test only a small uplift was observed. The developments of the cracks in these specimens were smaller than the ones in the WE-series. Cracks did not appear until the cycles with large amplitudes (Figure 59). The sliding behaviour led to the failure of the bricks due to the developed tensile strength. An example of this is shown in Figure 60.

Figure 59: Cracks after 2nd Cycle with Amplitude 10 mm of WG5

Figure 60: Damaged Brick after the Test WG3

2.4.2. Maximum forces

Table 5 shows the maximal horizontal forces of the tests. The forces were determined only considering the cycles that were not influenced by the test setup (lack of space for movement of the vertical jacks). As explained in Section 2.1.4., the repetition specimens (containing a R in the label) were initially pushed away from the reaction wall, while the other specimens were initially pulled toward the reaction wall. By convention, the positive values represent the direction of initial movement, regardless of whether it was pushed or pulled. This has to be considered by comparing the Table 5. Furthermore, the amplitude of the last completely conducted cycle is listed in the table.

Specimen	H_{max} [kN]	H_{min}[kN]	a_{max} [mm]
W0R	48.6	-55.4	20
WE3R	39.1	-41.1	20
WE5R	46.2	-47.0	20
WE10	45.2	-46.3	15
Mean	43.5	-44.8	
WG3	46.2	-46.5	20
WG5	49.3	-46.8	30
WG10	49.3	-46.8	30
Mean	48.3	-46.7	

Table 5: Extreme Values

All specimens with the built-in granulate rubber soft-layer had a similar horizontal load resistance. Only the specimen with the thinnest layer attained a resistance below the mean. The level of shear strength of the specimen with built-in granulate rubber material is higher than the one of the specimen with built-in extruded elastomer soft-layers. For the WE-series, the specimen with the thinnest built-in membrane developed the lowest horizontal strength.

In comparison with the control specimen, the wallets containing a soft-layer have a somewhat smaller horizontal load strength, especially for the specimens with built-in extruded elastomers. The critical force for a rigid body motion due to rocking was computed as 52.7 kN (see Appendix A). This value is valid for a rigid body with the actual geometry and the point of equilibrium right at the edge of the wall. This value fits quite well to the mean value of the maximum occurring horizontal forces during the test W0R (52 kN).

2.4.3. Backbone curves

The backbone curves were considered for the observation of the strength development over the cycles. The WE-series specimens have similar initial stiffness, as can be seen in Figure 61, while the initial stiffness of the WG-series specimens are more widely distributed (Figure 62). The specimens with built-in rubber granulate soft-layers had similar peak strengths (41 – 43.5 kN), the wallets with built-in extruded elastomer instead had more widely distributed peak strength (36.5 – 43.5 kN).

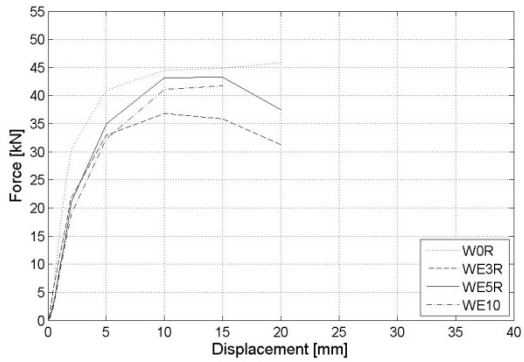

Figure 61: Comparison of the Backbone Curves WE-Series

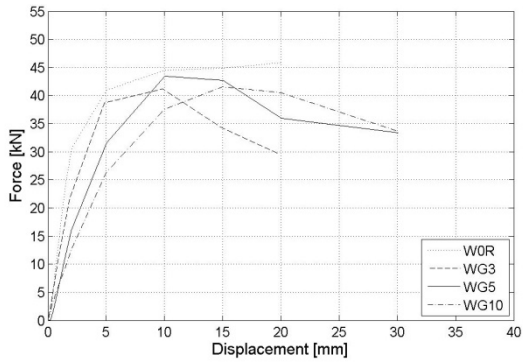

Figure 62: Comparison of the Backbone Curves WG-Series

2.4.4. Damage

The damage states of the soft-layer membranes after the tests are related to the response mechanism developed by the specimens and the amount of energy they dissipate during the tests. The soft-layers of the WE-series are hardly damaged (Figure 63), while the ones of the WG-series experienced extensive damage (Figure 64). The soft-layers of all specimens after the tests are shown in Figures 34-36 and Figures 52-54 in Section 2.3.2 and Section 2.3.3 for WE and WG specimens, respectively.

Figure 63: Damaged Soft-Layer WE3R

Figure 64: Damaged Soft-Layer WG3

As stated in the Section 2.3, the difference between the damping ratios of the first and the second cycle was small for all specimens. The damping for the WG-series is significantly higher than that for the WE-series. The following plots compare the damping ratios in one diagram for the first cycles and in another for the second cycles at the same amplitude amplitude. This is done for both types of built-in membranes.

The thickness of the soft-layer has a small influence on the damping ratio of the specimens with the extruded polymer membrane. This can be seen for the first cycle damping (Figure 65) and also for the second one (Figure 66). By considering the damping ratios of the WG-series (Figure 67 and 68), the

thinner soft-layers dissipate significantly more energy than the one with 10 mm. The damping ratios stayed almost constant for the WG-series between the first and the second cycle.

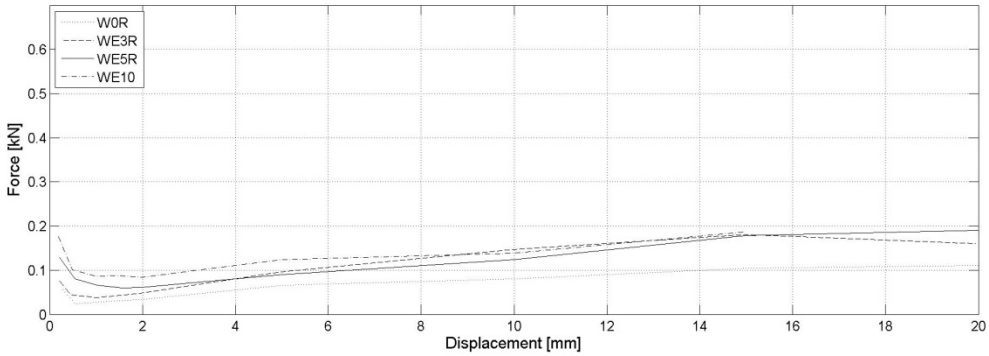

Figure 65: Comparison First Cycle of the Damping Ratio WE-Series

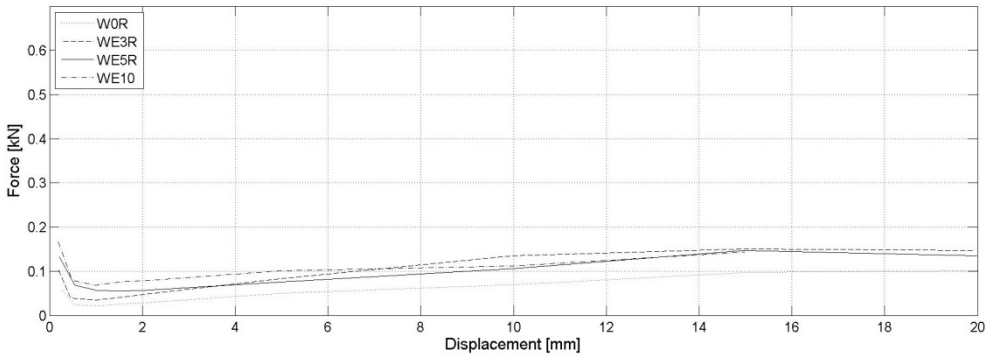

Figure 66: Comparison Second Cycle of the Damping Ratio WE-Series

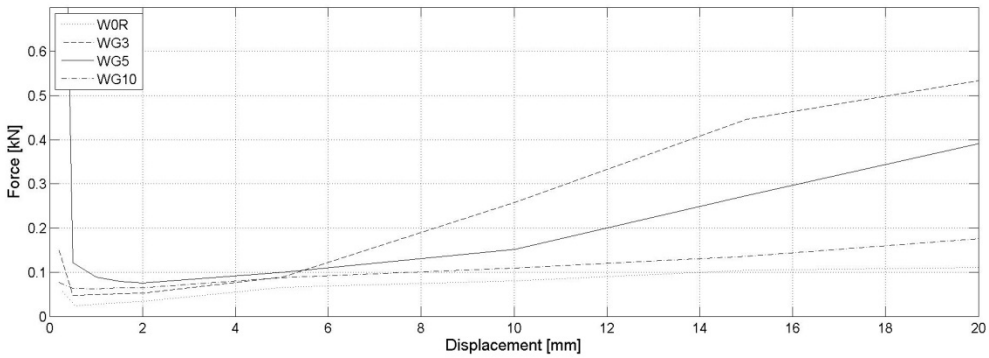

Figure 67: Comparison First Cycle of the Damping Ratio WG-Series

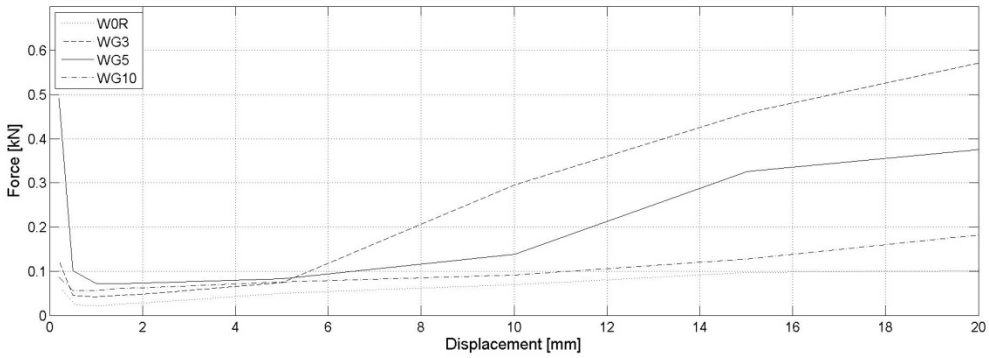

Figure 68: Comparison Second Cycle of the Damping Ratio WG-Series

3. Modelling Part

The main source of this chapter is OpenSees, 2013.

3.1. OpenSees

OpenSees (Open System for Earthquake Engineering Simulation) is a finite element method (FEM) software, developed at the University of California, Berkeley Pacific Earthquake Engineering Research Center (PEER) (PEER, 2013).

Because the existing software in the discipline of dynamic modelling was not satisfying, PEER supported the development of an open-source software. The open-source software allows the users to see the source code and to contribute it for everyone's benefit. With OpenSees the user can model geotechnical and structural problems dynamically in one application.

The programming language is the technical program language (tcl). The language library contains an OpenSees extension in addition to the ordinary tcl-commands, in which several modules for specific utilizations are supplied. These extensions are programmed in C++.

The compilation of the tcl-scripts can be done in an editor. By invoking these files in OpenSees, the scripts can be run. The outputs are specified in the tcl-scripts and are recorded in separate files, to be processed with an adequate program subsequently.

3.2. The Model

Building a model is one of the first steps in creating an OpenSees simulation. Independent modules are defined and tagged. Through these tags, they can be allocated to the location they are needed. Elements can be put together by referring to previously defined nodes, and the properties of the elements can be defined by referring to the desired materials tags.

The modules used in this thesis are presented in the following paragraphs.

3.2.1. BeamColumnJoint Element

The squat geometry of the specimens led to shear dominated behaviour in the walls. The soft-layers introduced additional sliding and rocking behaviours. In these circumstances, the existing OpenSees BeamColumnJoint element is appropriate.

As the name says, this command was developed for modelling the conjunction between beams and columns in a framework. The element is a rectangular shear panel possessing three springs at each face. For the shear panel the developer made the assumption that it can only deform in shear (Lowes & Mitra, 2004).

Two of the springs, located at the edges of each face, are designated for capturing the bending behaviour. The third spring acts in the orthogonal direction on each face, and it is responsible for transferring the shear force (see Figure 69). The intension by using this element was that the springs at the edges were appropriate to capture the rocking in the walls and the shear spring can capture the sliding.

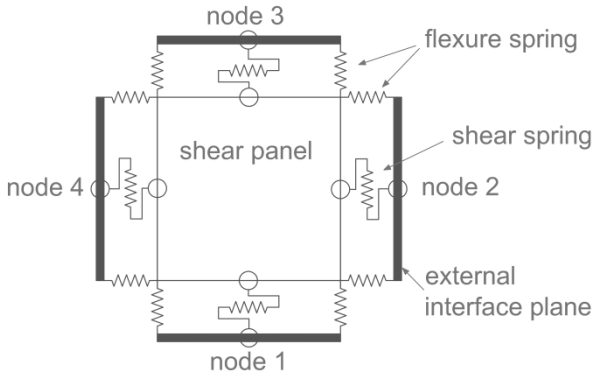

Figure 69: General BeamColumnJoint Element

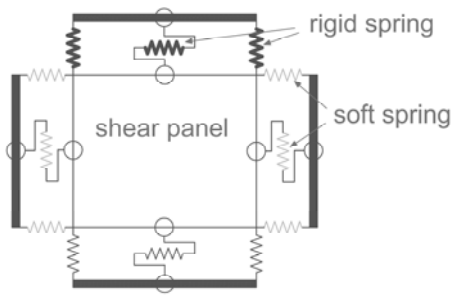

Figure 70: Adjusted BeamColumnJoint Element

At the outer sides, the springs are fixed at external interface planes. These planes allow connecting the BeamColumnJoint element to other elements. The springs and the external interface planes have no length, so they will not influence the geometrical attributes of the model.

The OpenSees command for the BeamColumnJoint element is shown below, and the input parameters are explained in Table 6.

element beamColumnJoint $eleTag $Nd1 $Nd2 $Nd3 $Nd4 $Mat1 $Mat2 $Mat3 $Mat4 $Mat5 $Mat6 $Mat7 $Mat8 $Mat9 $Mat10 $ Mat11 $Mat12 $Mat13 <$eleHeightFac $eleWidthFac>

element BeamColumnJoint	Command for calling the appropriate element
eleTag	Tag of the element
Ndi	Node names, defined anticlockwise
Mat1 – Mat12	Material tags of previously defined materials, for the springs
Mat13	Material tag of previously defined material, for the shear panel
eleHeightFac	Factor of the element height, for changing the position of lateral flexure positions
eleWidthFac	Factor of the element width, for changing the position of flexure springs positions of the top and the bottom

Table 6: Explanation BeamColumnJoint Command

The properties of the components of this element have to be allocated according to the attributes of the specimens. The shear panel (Mat13 of Table 6) was designated to represent the masonry part of the wallets between the polymer membrane and the beam above the masonry. The three springs at the bottom (Mat1-3) were aimed to represent the soft-layer. These four components of the model are the most important ones for simulating the behaviour of the wallets.

Because the lateral external interface planes are not connected to anything than the shear panel, the lateral springs (Mat4-6 and Mat10-11) do not influence the results. Accordingly, the properties were taken to be very soft (soft springs of Figure 70).

While the lateral spring properties are not used for this model, the springs at the top of the shear panel (Mat7-9) must transfer the loads without any deformation, so they are assigned rigid properties (rigid springs in Figure 70).

3.2.2. Additional Elements

One additional element was located above and one below the BeamColumnJoint element to represent the top beam and the baseplate with the first course of bricks, respectively. Both of these elements had to transfer the forces with small deformations, so they were modelled using the same properties as the springs at the top of the shear panel. The element command is shown below.

element elasticBeamColumn $eleTag $iNode $jNode $A $E $Iz $transfTag <-mass $massDens>

element elasticBeamColumn	Command for calling the appropriate element
eleTag	Tag of the element
iNode	Node tag at one side of the element
jNode	Node tag at the other side of the element
A, E, Iz	Attributes (Area, modulus of elasticity & moment of inertia) of the element
transfTag	Tag for a coordinate-transformation
-mass massDens	Element mass density (per unit length)

Table 7: Explanation elasticBeamColumn Command

3.2.3. Composition of the Elements

For modelling the test setup with the wallets, six nodes were used (Figure 72). Node 1 is located at the bottom below the "baseplate". At this node all of the three degrees of freedom (F_x, F_y and M_z) are fixed, so the beam below the shear panel is clamped in the foundation slab. The length of this beam is 0.26 m as result of the sum of the baseplate thickness (0.5 m), the height of one course of bricks (0.2 m) and the thickness of the mortar bed (0.01 m).

Node 6 is situated on the opposite side of the model, at the top, and its degrees of freedom are unconstrained. Nodes 2, 3, 4, and 5 are located around the BeamColumnJoint element. Node 2 is defined to be the connection between the base beam and the interface plane below the shear panel. Node 3, 4, and 5 are defined in a counterclockwise direction around the BeamColumnJoint element. The link between the top beam and the top, external interface plane (node 5) works in the same manner as node 1. The whole model can be considered as a cantilever consisting of different beams with different properties. Figure 71 shows a drawing of the test setup in the laboratory for comparison with the FE-model in Figure 72.

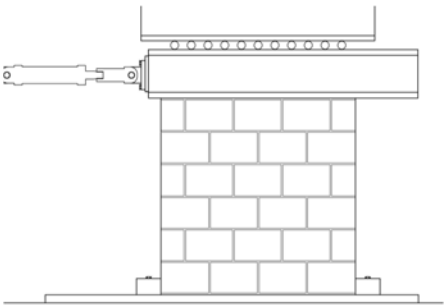

Figure 71: Test Setup for the Experimental Tests

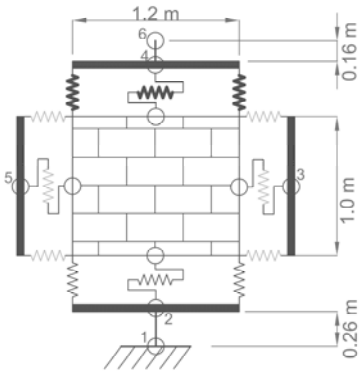

Figure 72: FE- Model

3.3. Materials

The materials give the different elements their properties. An existing material library in OpenSees offers the users a many choices of materials. The number of input parameters for characterizing a material varies significantly. In the simplest case, only one parameter is used, while for a complicated case, many parameters are used. By considering each element of the model independently, the allocation of the appropriate materials was done. In the next pages the selected material types and the explanations are presented.

3.3.1. Shear Panel

As can be seen in the experimental part of this thesis, either the failure occurs in the soft-layer joint (sliding) or because of the geometry (rocking). Because of this, the shear panel never reaches its strength level, so it can be modelled as a linear elastic material. This assumption is not physically correct because the shear panel cracks in the tests, but considering the higher strength of the masonry compared to the other materials, the elastic material is appropriate. However, the FE-model is not able to dissipate energy in the shear panel this way.

The schematic of the OpenSees material is shown in Figure 73 and an example output of the model is displayed in Figure 74.

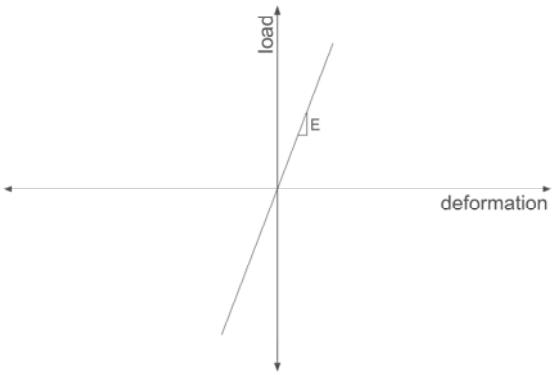

Figure 73: Schematic of the Elastic Material

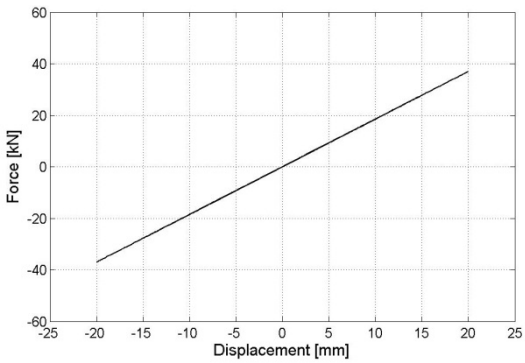

Figure 74: Example Output for the Elastic Material

For characterizing the elastic material properties only one parameter is needed, namely the modulus of elasticity E. The command is shown below and its explanation is shown in Table 8.

uniaxialMaterial Elastic $matTag $E <$eta>

uniaxialMaterial Elastic	Command for calling the appropriate material
matTag	Tag of the material
E	Modulus of elasticity
eta	Damping tangent (optional)

Table 8: Explanation uniaxialMaterial Elastic Command

3.3.2. Flexure Springs

In the next paragraphs, the springs refer to the ones at the bottom of the BeamColumJoint element.

The flexure spring have two different tasks: They have to transfer the vertical load and the bending moment to the foundation. However, the joint is not able to transfer tension, so uplift can occur.

Considering this, an elastic-no tension (ENT) material was chosen for these two springs. In the following figures the schematic of the material (Figure 75) and an example OpenSees plot (Figure 76) are shown. In the example output the curve is nonlinear because, the model was rocking during the analysis.

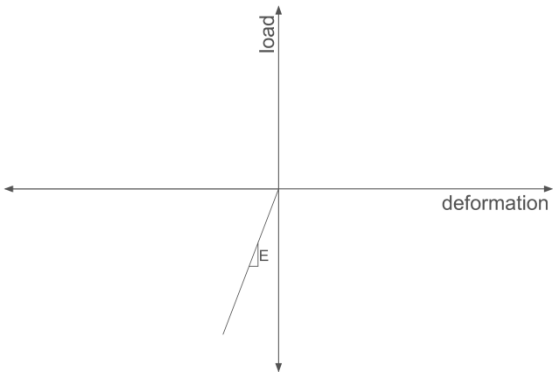

Figure 75: Schematic of the Elastic-No Tension Material

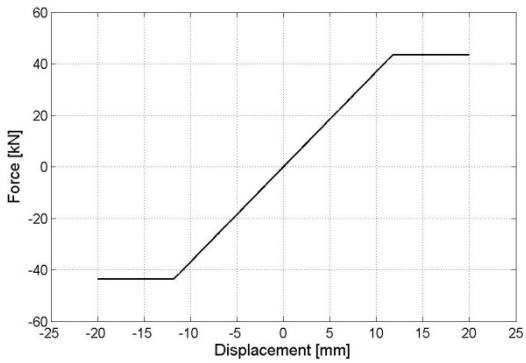

Figure 76: Example Output for the Elastic-No Tension Material

The number of required input parameters is also confined to one parameter, the elastic modulus E. The command is shown below and its explanation is shown in Table 9.

uniaxialMaterial ENT $matTag $E

uniaxialMaterial ENT	Command for calling the appropriate material
matTag	Tag of the material
E	Modulus of elasticity

Table 9: Explanation uniaxialMaterial ENT Command

3.3.3. Shear Spring

In the FE-model, the hysteretic behaviour is mainly ensured by the properties of the shear spring. The OpenSees pinching4 material is used for simulating this behaviour. This material allows changing the material behaviour in different ways. Figure 77 shows an overview of the material and in Figure 78 shows the output from OpenSees.

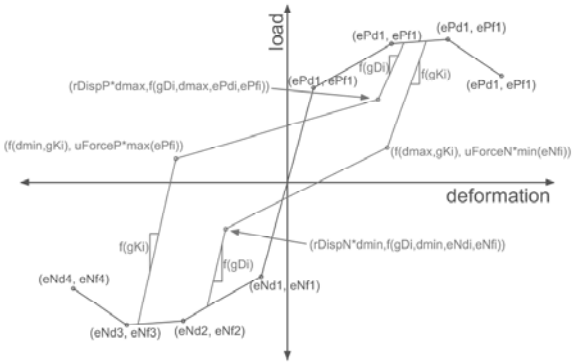

Figure 77: Schematic of the Pinching4 Material

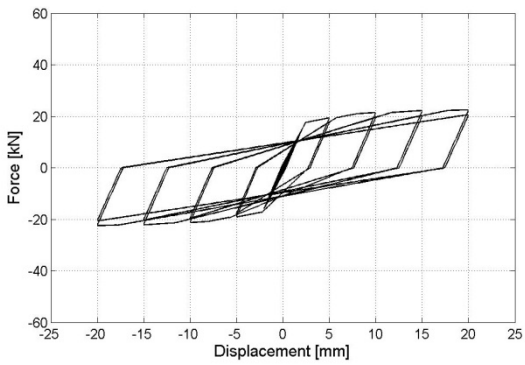

Figure 78: Example Output for the Pinching4 Material

The adjustment of the correct shape of the hysteresis has to be done with a total of 39 parameters (see command below). A response envelope is defined with 16 parameters in the form of different forces and displacements. In case of a cyclic loading, like in the present one, the unloading and reloading path can be adjusted by changing another 6 parameters. These 22 parameters are shown in Figure 77 and explained in Table 10 (Lowes & Mitra, 2004).

uniaxialMaterial Pinching4 $matTag $ePf1 $ePd1 $ePf2 $ePd2 $ePf3 $ePd3 $ePf4 $ePd4 <$eNf1 $eNd1 $eNf2 $eNd2 $eNf3 $eNd3 $eNf4 $eNd4> $rDispP $rForceP $uForceP <$rDispN $rForceN $uForceN > $gK1 $gK2 $gK3 $gK4 $gKLim $gD1 $gD2 $gD3 $gD4 $gDLim $gF1 $gF2 $gF3 $gF4 $gFLim $gE $dmgType

uniaxialMaterial Pinching4	Command for calling the appropriate material
matTag	Tag of the material
Pfi, Nfi	Forces for the response envelope
Pdi, Ndi	Displacements for the response envelope
rDispP, rDispN	Value for adapting the displacement of the point where reloading occurs
rForceP, rForceN	Value for adapting the force of the point where reloading occurs
uForceP, uForceP	Value for adapting the force of the point where reloading begins
gKi, gDi, gFi, gE, dmgType	Damage, explained in Table 11

Table 10: Explanation uniaxialMaterial Pinching4 Command

Furthermore three different types of damages can be applied. There is unloading stiffness degradation, reloading stiffness degradation and strength degradation. For each of these damages types, five input parameter have to be specified. In the Table 11 the consequences of the different modes are explained. In this table also the supplementary parameters for characterizing the damage are also listed.

Input Parameters	Function	Formulas	Schematic
gK1 gK2 gK3 gK4 gKLim	Values controlling the cyclic degradation model for unloading stiffness degradation	$\delta ki = (gK1 \cdot (\tilde{d}_{\max})^{gK3} + gK2 \cdot gE^{gK4}) \leq gKLim$ $\tilde{d}_{\max} = \max\left[\frac{d_{\max,i}}{def_{\max}}, \frac{d_{\min,i}}{def_{\min}}\right]$ $k_i = k_0 \cdot (1 - \delta k_i)$	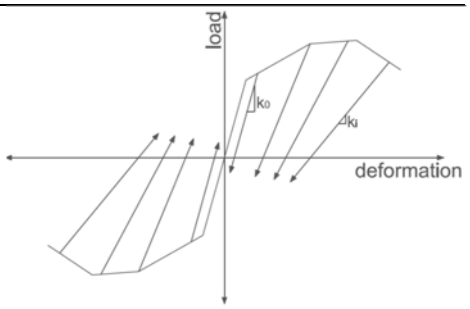
gD1 gD2 gD3 gD4 gDLim	Values controlling cyclic degradation model for reloading stiffness degradation	$\delta d_i = (gD1 \cdot (\tilde{d}_{\max})^{gD3} + gD2 \cdot gE^{gD4}) \leq gDLim$ $\tilde{d}_{\max} = \max\left[\frac{d_{\max,i}}{def_{\max}}, \frac{d_{\min,i}}{def_{\min}}\right]$ $d_{\max,i} = d_{\max,0} \cdot (1 + \delta d_i)$	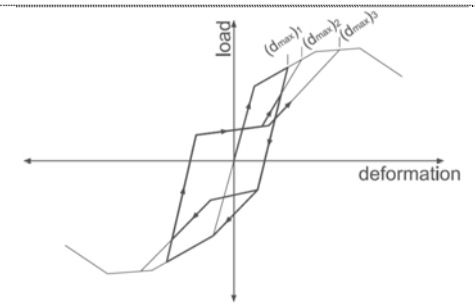
gF1 gF2 gF3 gF4 gFLim	Values controlling cyclic degradation model for strength degradation	$\delta f_i = (gF1 \cdot (\tilde{d}_{\max})^{gF3} + gF2 \cdot gE^{gF4}) \leq gFLim$ $\tilde{d}_{\max} = \max\left[\frac{d_{\max,i}}{def_{\max}}, \frac{d_{\min,i}}{def_{\min}}\right]$ $(f_{\max})_i = (f_{\max})_0 \cdot (1 - \delta f_i)$	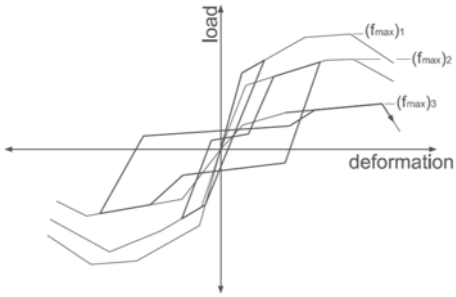
gE	Value used to define maximum energy dissipation under cyclic loading. Total energy dissipation capacity is defined as this factor multiplied by the energy dissipated under monotonic loading.	$gE = \left(\frac{E_i}{E_{\text{monotonic}}}\right)$	
dmgType	String to indicate type of damage (option: "cycle", "energy")		

Table 11: Explanation Damage Pinching4 Material

3.3.4. Additional Materials

In the previous chapters the initially designated materials were presented. In the case of the appearance of rocking, the resultant bilinear shape of the hysteresis was unsatisfactory. Based on this, some adaptions were made to the FE-model. The elements of the adapted model have different material properties.

3.3.4.1. Self-Centering Material

To simulate the rocking performance, the self-centering material of the OpenSees was used. This type of material was developed to imitate the behaviour of a self-centering bearing. The hysteresis is flag-shaped, and the material allows for making some adaptions, as shown in the explanation of the command.

The schematic of the material (Figure 79) and an example plot (Figure 80) are shown below.

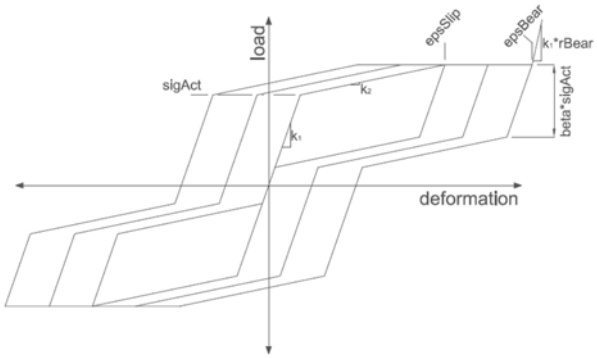

Figure 79: Schematic of the Self-Centering Material

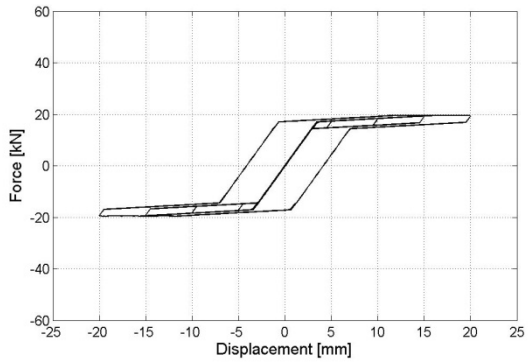

Figure 80: Example Output for the Self-Centering Material

Although this adapted model lacks complete physical correctness, the behaviour of the system can be met quite well.

The command and its explanation (Table 12) are shown below.

uniaxialMaterial SelfCentering $matTag $k1 $k2 $sigAct $beta <$epsSlip> <$epsBear> <rBear>

uniaxialMaterial SelfCentering	Command for calling the appropriate material
matTag	Tag of the material
k1	Initial stiffness
k2	Post-activation stiffness
sigAct	Activation stress/force (transition k1 to k2)
beta	Height of the flag, ratio of forward and reverse activation stress/force
epsSlip	Slip strain/deformation
epsBear	Bearing strain/deformation
rBear	Ratio of bearing stiffness to k1

Table 12: Explanation uniaxialMaterial SelfCentering Command

3.3.4.2. Hysteretic Material

The hysteretic material command gives similar results to the Pinching4 material, but fewer parameters are needed (see command below).

This is advantageous for the combination (as a parallel material, see next paragraph) with the Self-centering material. Otherwise the model would become too complex to fit the results efficiently.

Figure 81 shows the schematic of the material and Figure 82 shows an appropriate example plot.

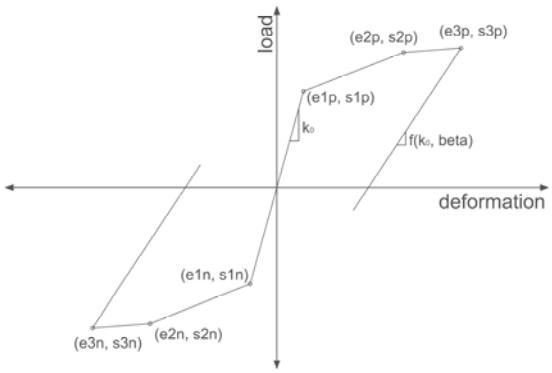

Figure 81: Schematic of the Hysteretic Material

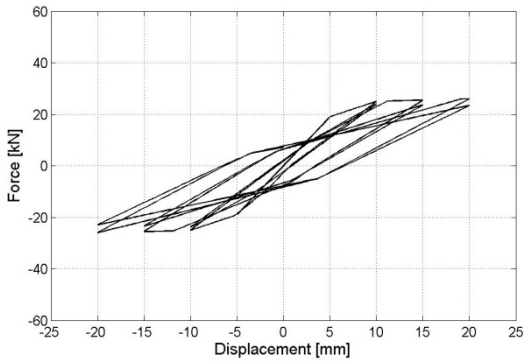

Figure 82: Example Output for the Hysteretic Material

Below the OpenSees command is shown. In Table 13 the explanations of it are listed.

uniaxialMaterial Hysteretic $matTag $s1p $e1p $s2p $e2p <$s3p $e3p> $s1n $e1n $s2n $e2n <$s3n $e3n> $pinchX $pinchY $damage1 $damage2 <$beta>

uniaxialMaterial Hysteretic	Command for calling the appropriate material
matTag	Tag of the material
sip /sin	Stresses/forces of the positive/negative response envelope
eip /ein	Strains/deformations of the positive/negative response envelope
pinchx	Pinching factor for strain during reloading
pinchy	Pinching factor for stress during reloading
damage1	Adjusting the damage due to ductility
damage2	Adjusting the damage due to energy
beta	Adjusting the unloading stiffness

Table 13: Explanation uniaxialMaterial Hysteretic Command

3.3.4.3. Parallel Material

Because no mixed behaviour of rocking (elastic-no tension material) and sliding (pinching4 material) can occur in OpenSees, a different option was needed to simulate the hysteresis best (see Section 3.5.2).

The decision was made to simulate the behaviour of the model for the specimen with a predominant rocking performance with a parallel material. The shear spring possessed this material instead of the Pinching4 material. Furthermore, the flexure springs were assigned an elastic material instead of the elastic-no tension one, so the rocking failure could not occur. With these changes, the model was no longer physically correct, but the material could be calibrated to reach a good fit with the test results. Because the output from using the self-centering material for the shear spring was unsatisfactory, a parallel combination was made with the self-centering material and the hysteretic material. For combining materials, OpenSees offers two options: One is to use a parallel material for which the strains are equal while the stresses are additive. The other option is a series material for which the curves are put together in the opposite way.

For reaching an appropriate shape of the hysteresis curve, a parallel material of the OpenSees library was used. In Figure 83 an example for a parallel material is shown.

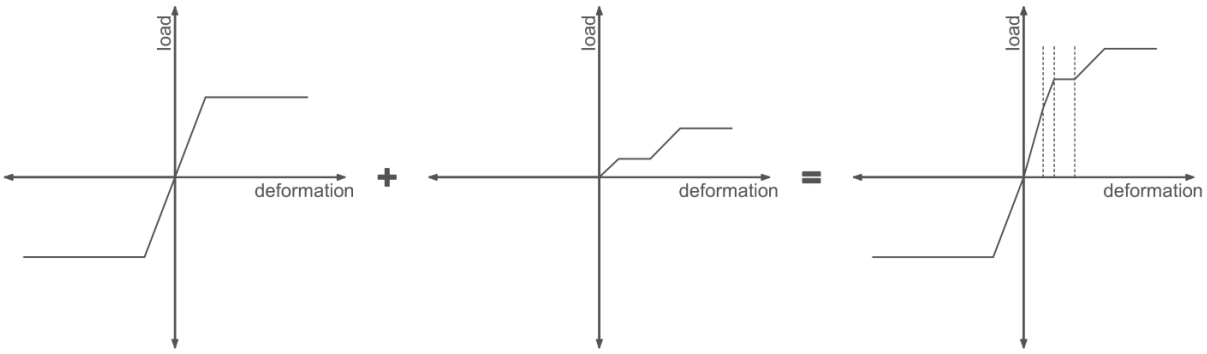

Figure 83: Schematic of an Example for a Parallel Material

The command for a parallel material is very simple:

uniaxialMaterial Parallel $matTag $tag1 $tag2 ...

The explanation of the command is shown in Table 14.

uniaxialMaterial Parallel	Command for calling the appropriate material
matTag	Tag of the material
tagi	Material tags of the materials wanted to be combined

Table 14: Explanation uniaxialMaterial Parallel Command

3.4. Analysis

In the following chapter the parameters for the OpenSees model are defined.

3.4.1. Loads

The loads and displacements applied to the OpenSees model matched those used for the tests in the laboratory. In case of the vertical load, the same force (100.9 kN) was applied to the numerical model in the y-direction. The location where the load was applied was on the top of the top beam (Figure 84). Dead loads were not applied in the FE-model.

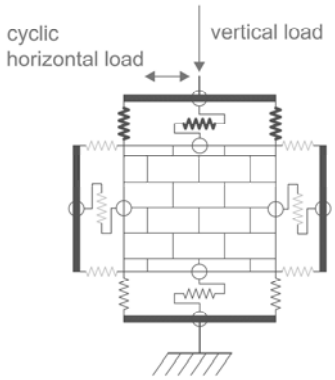

Figure 84: FE-Model with Loads

In the lab, the horizontal motion was applied with displacement control. The same displacement history was used in OpenSees, generated with the script `LibGeneratePeaks_sine.tcl`. All tcl-scripts are on the compact disc in the appendix. The displacement history is shown in Figure 85.

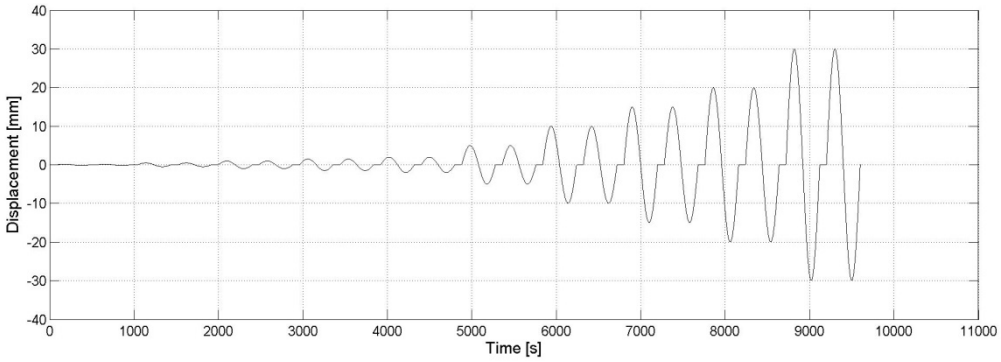

Figure 85: Applied Displacement History to the FE-Model

3.4.2. Recorder

Before running the analysis, the desired output has to be defined. This can be done with the recorder command, by setting the desired location and type (force or displacement and in which direction).

3.4.3. Analysis Parameters

The model which is used to simulate the behaviour of the wallets with soft-layer has to run two different analyses. The first analysis applied the vertical load, and the second one applied the horizontal displacement history. In Table 15, the chosen analysis parameters for the vertical load analysis are briefly described with their functions. In Table 16, the parameters for the horizontal displacement history analysis are described.

Constraints Plain	The required type of constraints is dependent of the model. It determines how the constraints equations are enforced in the analysis. For this simple model the type plain is appropriate.
Numberer Plain	Constructs the degree-of-freedom (DOF) -Numberer object. This determines the mapping between equation numbers and DOF, how DOF are numbered. The constraints have to be homogenous for single point constraints or the constraint matrix has to be equal to the identity for multi-point constraints
System BandGeneral	Command used for constructing the linear system of equation object. The Type BandGeneral is utilized for banded profiles with linear systems of equation objects.
Test EnergyIncr	Conduct a convergence test using the dot product of the solution vector and norm of the right hand side of the matrix equation. Doing this, it can determine if convergence has been reached.
Algorithm Newton	Command used to construct a Solution Algorithm. In this case the Newton Algrithm was used.
Integrator LoadControl	Defines the integrator object. It defines the predictive step for time steps and determines the force increments to be finally at the prescribed value.
Analysis Static	Command which defines the type of analysis. In this case a static analysis is appropriate.

Table 15: Analysis Parameters for Vertical Load Analysis

Constraints Plain	The required type of constraints is dependent of the model. It determines how the constraints equations are enforced in the analysis. For this simple model the type plain is appropriate.
Numberer RCM	Constructs the degree-of-freedom (DOF) -Numberer object. This determines the mapping between equation numbers and DOF, how DOF are numbered. RCM uses the reverse Cuthill-McKee scheme as basis for doing that.
System BandSPD	Command used for constructing the linear system of equation object. The type BandSPD is utilized for banded profiles with symmetric positive definite matrices.
Test NormDispIncr	Conduct a convergence test using the relative of the solution vector of the matrix equation. Doing this, it can determine if convergence has been reached.
Algorithm Newton	Command used to construct a Solution Algorithm. In this case the Newton Algrithm was used.
Integrator DisplacementControl	Defines the integrator object. It defines the predictive step for time steps and determines the displacement increments to be finally at the prescribed value.
Analysis Static	Command which defines the type of analysis. In this case a static analysis is appropriate.

Table 16: Analysis Parameters for Lateral Load Analysis

With the command analyze the analysis is run and the output is saved to the previously defined recorder files.

3.5. Simulations and Results

For running the model, four tcl-scripts are required: The file `LibGeneratePeaks_sine.tcl` creates the displacement history, the file `procsineRC.tcl` runs the analysis of the horizontal loading and the file `masonry.wall.withSL.tcl` defines the general model parameters (geometry, elements, materials, forces …) and runs the analysis of the vertical loading. The fourth tcl-file, `SL_mat_par.tcl`, was created in Matlab to efficiently adjust the input parameters of the materials. The scripts are included on the compact disc in the appendix.

The different scripts are linked, so only the main file (`masonry.wall.withSL.tcl`) has to be invoked in the OpenSees executor.

The output of the OpenSees model will be discussed next. The results of the FE-model are compared to the test results of the specimen tested in the lab.

3.5.1. Input Parameters

The geometry of the components can be seen in Figure 72. The properties of the rigid parts of the model, namely the top beam, the base plate, and the springs at the top of the BeamColumnJoint element, were kept unaltered (1.e18 N/m).

Initially, the stiffness of the shear panel was estimated by the data from the control specimen (W0R). Since rocking occurred, the stiffness did not representative the properties of the masonry but rather depended on the geometry.

Instead, the stiffness of the shear-panel was determined from the data of Salmanpour et al., 2013. Although the masonry tests which were conducted in this work had different dimensions, there were many similarities: the specimen was built with the same type of brick (Swissmodul B15/19), the aspect ratio was similar (0.94 compared to 1.0), the vertical loading was the same (10 % of the vertical load strength) and the horizontal load was also applied with displacement control. The test setup in the work of Salmanpour et al., 2013 prevented the occurrence of rocking. The elastic stiffness of the shear panel was determined from the force displacement diagram from this data and computed to be 4.1e7 N/m.

3.5.2. Problems with the Model

As already mentioned, there were convergence difficulties with combining different parts of the model with their appropriate material properties. The difficulties will be explained in this chapter.

For the stiffness of the shear panel the value presented in the previous section was chosen. With this assumption, the remaining parts of the model to be defined were the flexure springs and the shear spring, representing the behaviour along the soft-layer. In order to test the rocking performance of the model, the Elastic-No Tension material was assigned to the flexure springs and the elastic material to the shear spring. Figure 86 shows the output of the rocking behaviour. The model is very sensitive to the inserted parameters, and for small changes, the simulation failed due to convergence problems. The values inserted for a successful simulation of this behaviour are summarized next to the plot in Table 17.

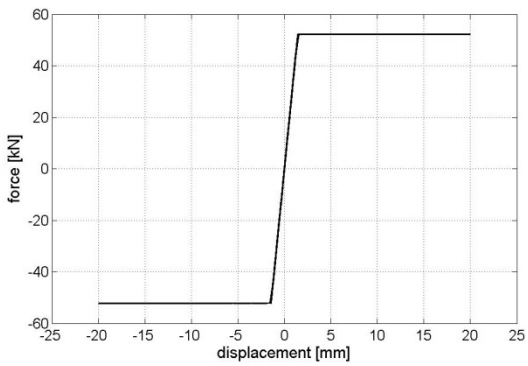

Figure 86: Testing of the Flexure Springs with ENT

Model part	Command	parameters
Shear panel	Elastic	E=4.1e7 N/m
Flexure spring	ENT	E=9.e8 N/m
Shear spring	Elastic	E=9.e8 N/m

Table 17: Input Parameters for Testing the Flexure Springs

In the next step the elastic material of the shear spring was replaced with the pinching4 material. With this combination, the model converged as long as the inserted response envelope of the pinchinig4 material did not cross the rocking force level (for this geometry 52.2 kN). The properties are given in Table 18 next to the output plot of OpenSees (Figure 87). For the pinching4 material only the parameters for the response envelope are shown (the damage and uForceP/N were set to 0.0, rDispP/N and rForceP/N to 1.0).

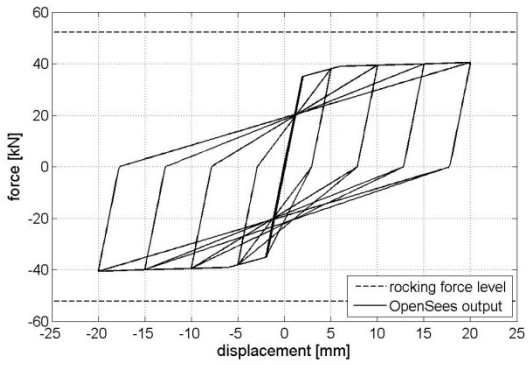

Figure 87: Testing of the Combinated Simulation: Flexure Springs (ENT) and Shear Spring (Pinching4)

Model part	Command	parameters
Shear panel	Elastic	E=4.1e7 N/m
Flexure spring	ENT	E=9.e8 N/m
Shear spring	Pinching4	ePf1=35 kN ePf2=39 kN ePf1=40 kN ePf2=42 kN ePd1=1 mm ePd2=5 mm ePd1=15 mm ePd2=30 mm

Table 18: Input Parameters for Testing the Combination

For the specimen W0R, rocking was the predominant behaviour in the experimental test. Based on this, the simulation in OpenSees can be done with a rigid shear spring. In Figure 88 you can see the hysteresis of the FE-model and also that of the experimental test of the control specimen. The model does not allow adapting the stiffness. The input parameters are shown in Table 19.

In Section 2.4.2., assuming the wall was rotating about its bottom corner, the rocking force level was calculated to be 52.7 kN (OpenSees estimated it to be 52.2 kN). In fact, the specimen actually rotated about a point a little more inside the wall. As an assumption, the center of rotation was chosen to be 0.1 m from the edge of the most lateral brick (see Appendix A). This assumption led to a dropping of the rocking force level to 43.9 kN by calculation. To account for this in the FE-model, the element width factor (eleWidthFac, Table 6 in Section 3.2.1.) of the BeamColumnJoint element was set to 5/6 (1 m/1.2 m). With this adaption each flexure spring moved in 1/12*(wall width) from the edges of the shear panel. The OpenSees simulation with the adapted positions of the flexure springs estimated the rocking force level to 43.5 kN.

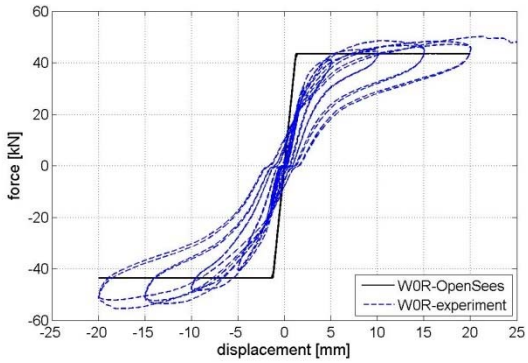

Figure 88: Comparision of the Hysteresis of W0R and the Simulation

Model part	Command	Parameters
Shear panel	Elastic	E=4.1e7 N/m
Flexure spring	ENT	E=9.e8 N/m
Shear spring	Elastic	E=9.e8 N/m

Table 19: Input Parameters for Simulation W0R with ENT and masonry stiffness

If the stiffness of the shear panel is replaced with a rigid one, the stiffness of the elastic-no tension material can be changed without convergence problems (Table 20). The hysteresis is shown in Figure 89.

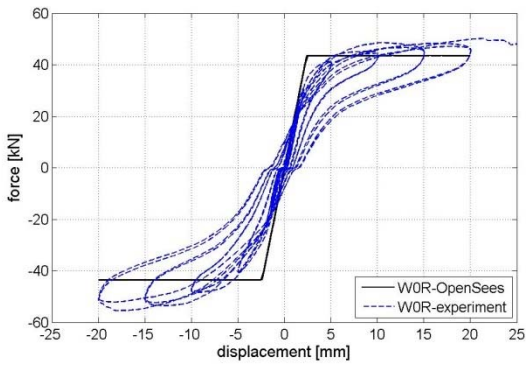

Figure 89: Comparison of the Hysteresis of W0R and Simulation with a Rigid Shear Panel

Model part	Command	Parameters
Shear panel	Elastic	E=1.e18
Flexure spring	ENT	E=5.e7
Shear spring	Elastic	E=9.e8

Table 20: Input Parameters for Simulation of W0R with ENT and big E for Shear Panel

It is apparent that the rocking behaviour does not simulate the experimental behaviour very well. The similarities are confined to the initial stiffness and the strength. In the simulation, no damping occurs, and because of that, the shapes of the hysteresis are not similar.

Considering these circumstances, the modelling of the specimens like this appeared to have no prospect of success, especially because the different parts of the model were difficult to combine without convergence problems.

3.5.3. Adapted Model

With some modifications to the model, the behaviour of the specimens of the experimental tests can be simulated. The adaptions include the replacement of the elastic-no tension materials of the flexure springs with an elastic material to prevent rocking. Thus the occurrence of convergence failure is minimized and the shear panel stiffness can be set to 4.1e7 N/m again. Also the material of the shear spring is replaced with one that is able to achieve similar attributes as the tested specimens.

Although the model is no longer physically correct, these changes were seen as the only way to simulate the performance of wallets.

In the following sections, the results of this model with the adapted attributes are presented. The maximum applied amplitude varied for the different specimens in the laboratory. For simulation, the same displacement history was applied to the FE-model as the different specimens underwent during the experiments.

3.5.4. Control specimen

To simulate the specimen with a predominant rocking behaviour, the parallel material was used. With the combination of the self-centering material and the hysteretic material, the hysteresis looks flag-shaped. The advantage of the parallel material compared to the self-centering material alone lies in its greater amount of adjustment options.

To compare the results of the FE analysis, the hysteresis (Figure 90), the backbone (Figure 91) curves and the damping ratios are shown (Figure 92 and 93). Additionally the areas of the hysteresis of the model and the experimental test were calculated (Figure 90).

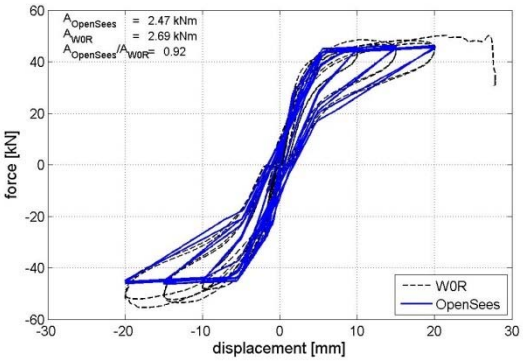

Figure 90: Comparison Hysteresis and Areas W0R

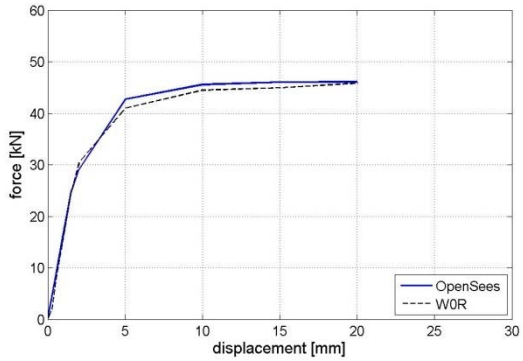

Figure 91: Comparison Backbone Curves W0R

The damping ratios calculated from the OpenSees data, shown in Figure 92 and Figure 93, fit the processed data of the experimental test well. For displacement amplitudes larger than 2 mm the differences are very small. The discrepancy between the OpenSees data and the test data for very small displacements is likely due to difficulties with measuring small displacements in the laboratory.

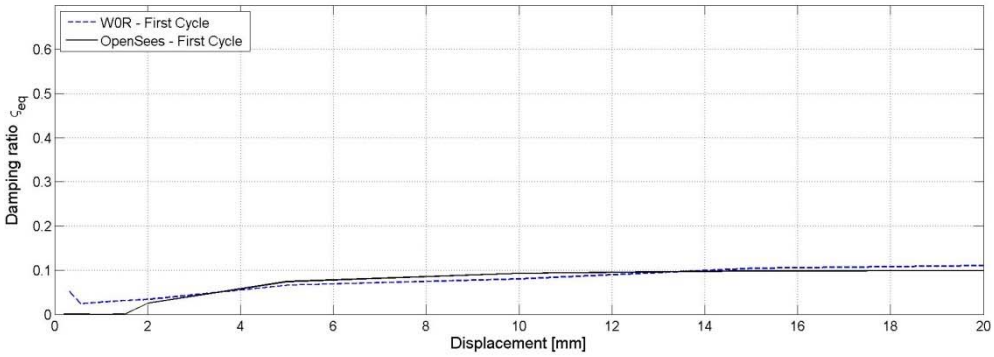

Figure 92: Comparison First Cycle's Damping Ratio W0R

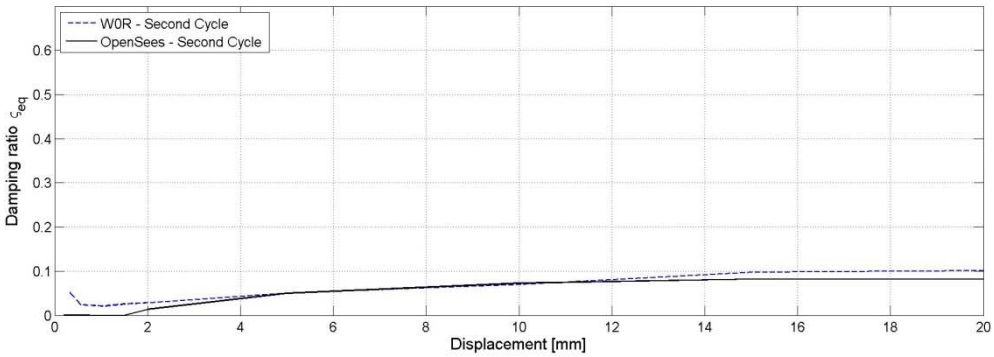

Figure 93: Comparison Second Cycle's Damping Ratio W0R

The input parameters of the materials for the simulation are described in the Table 21, following the plots of the WE-series.

3.5.5. WE-Series

The WE-series experienced a rocking behaviour like the control specimen. Based on this, the simulation was done with parallel material allocated to the shear spring. The flexure springs were assigned an elastic material.

3.5.5.1. WE3R

In Figure 94, the hysteresis is shown, and the ratio of the areas was calculated to be 0.84. The backbone curve of the simulation in Figure 95 fits well to the one of the experimental test.

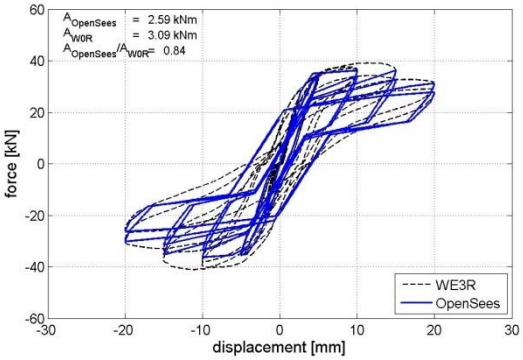

Figure 94: Comparison Hysteresis and Areas WE3R

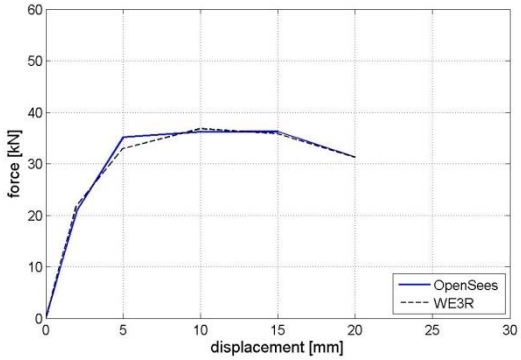

Figure 95: Comparison Backbone Curves WE3R

The damping ratios calculated from the OpenSees data for the first and the second cycles are shown in the figures below. They are consistently less than the damping ratios of the specimen WE3R for both cycles.

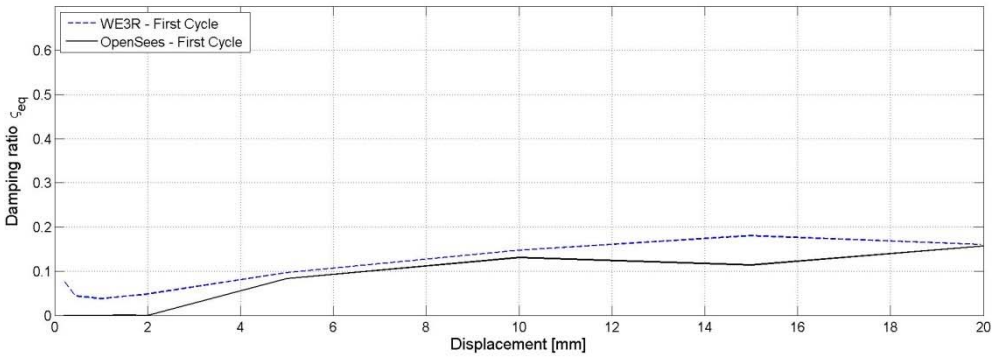

Figure 96: Comparison First Cycle's Damping Ratio WE3R

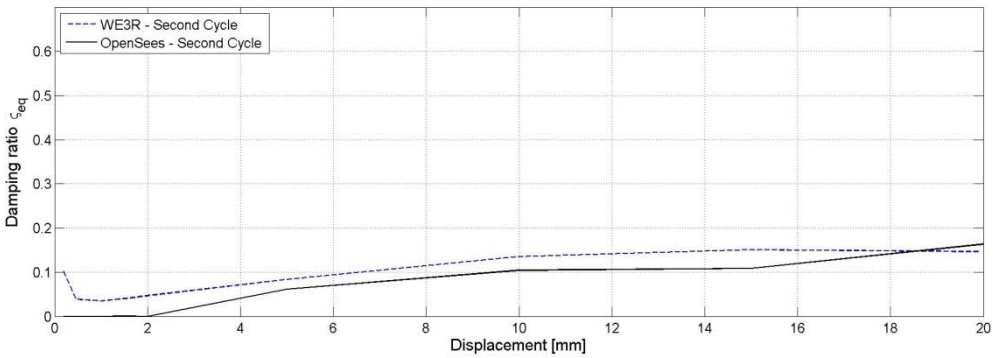

Figure 97: Comparison Second Cycle's Damping Ratio WE3R

The values of the input parameters are summarized in Table 21.

3.5.5.2. WE5R

Although the backbone curves (Figure 99) are very similar for WE5R, the areas in the hysteresis (Figure 98) differ by about 20 %.

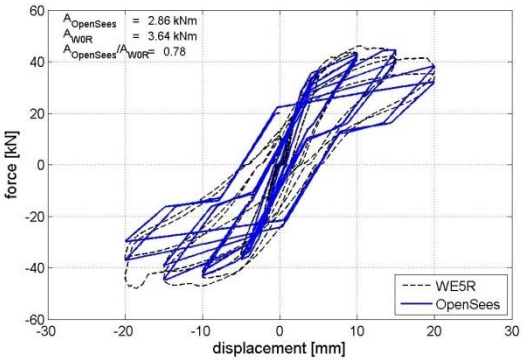

Figure 98: Comparison Hysteresis and Areas WE5R

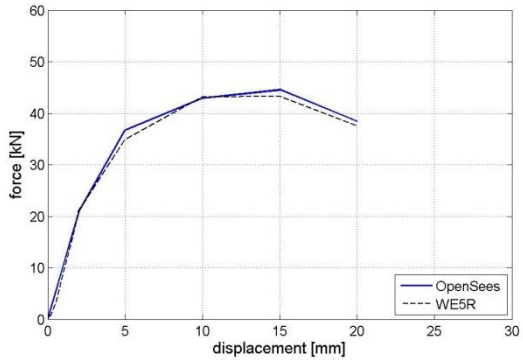

Figure 99: Comparison Backbone Curves WE5R

The damping ratios (Figure 100 and Figure 101) are not as similar to each other as they were in the previously presented simulations. The values computed from the OpenSees data are mainly less than the damping ratio of the experiment.

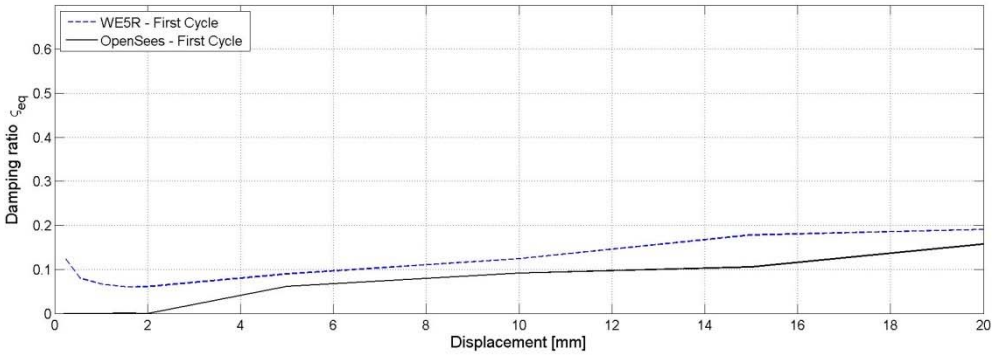

Figure 100: Comparison First Cycle's Damping Ratio WE5R

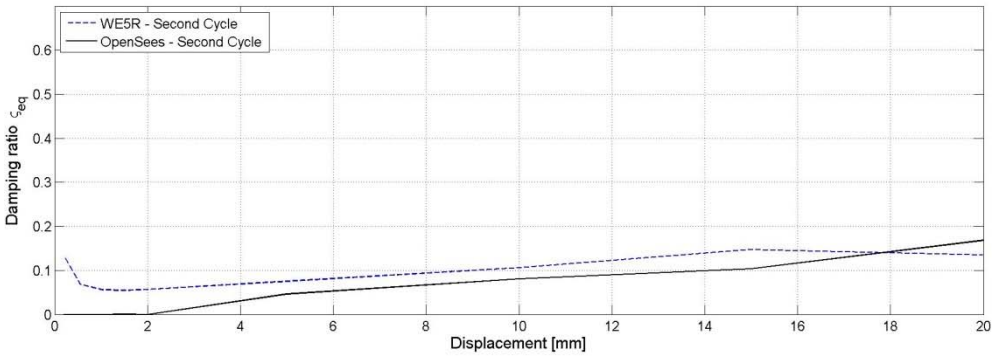

Figure 101: Comparison Second Cycle's Damping Ratio WE5R

In Table 21 the input parameters for the different materials of the FE-model are shown

3.5.5.3. WE10

The WE10 specimen was the experiment with the smallest peak displacement cycle amplitude, and the hysteresis has no distinct s-shape. So the modelling with the parallel material was hard. The hysteresis is shown in Figure 102 and the backbone curves are shown in Figure 103.

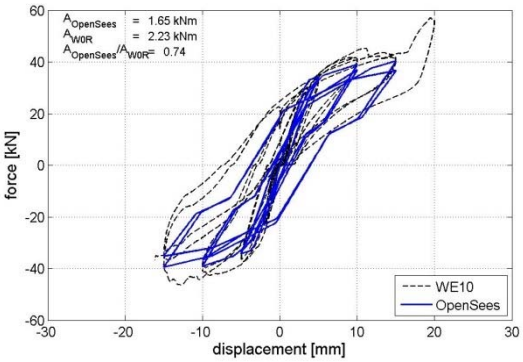

Figure 102: Comparison Hysteresis and Areas WE10

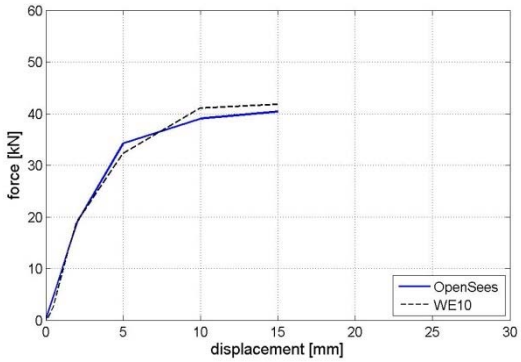

Figure 103: Comparison Backbone Curves WE10

The ratio of the areas (Figure 102) indicates the difference between the model and the experiment. The damping ratio plots (Figure 104 and Figure 105) emphasize this behaviour, especially for smaller cycles.

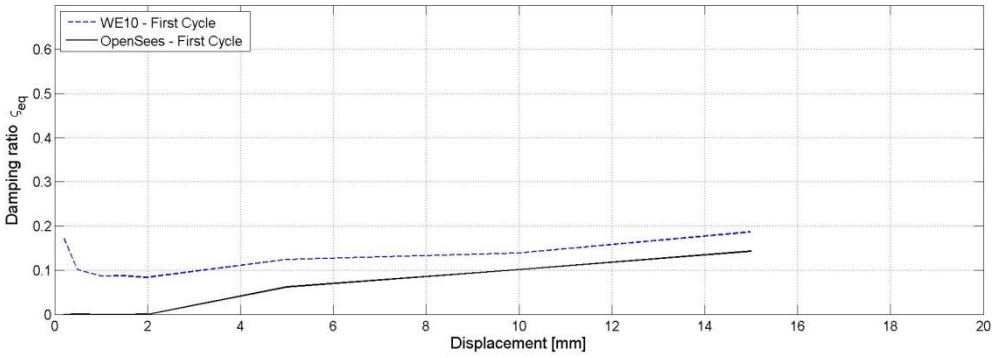

Figure 104: Comparison First Cycle's Damping Ratio WE10

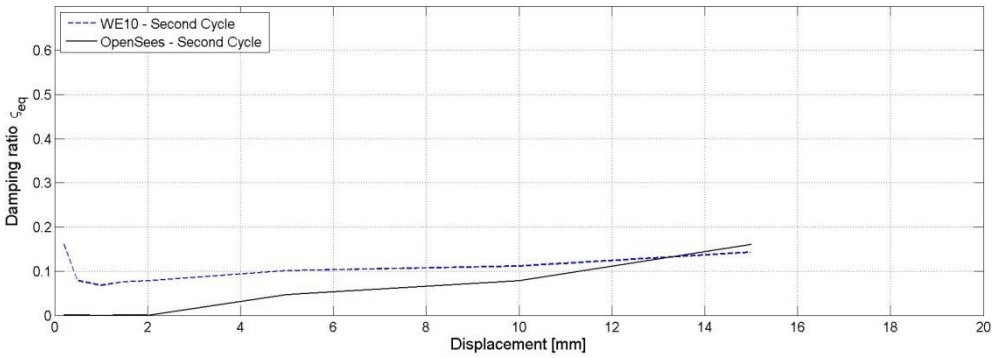

Figure 105: Comparison Second Cycle's Damping Ratio WE10

In the following table the input parameters for the simulation of the WE-specimens and the control specimen are summarized.

Component	Material		Input parameter	W0R	WE3R	WE5R	WE10
Shear panel	Elastic		E [N/m]	4.1e7	4.1e7	4.1e7	4.1e7
Flexure spring	Elastic		E [N/m]	5e18	5e18	5e18	5e18
Shear spring	Parallel	hysteretic	s1p [N]	22500	18000	18000	18000
			s2p [N]	24000	18100	28000	18500
			s3p [N]	24500	21000	29000	21000
			e1p [m]	0.001	0.002	0.002	0.0025
			e2p [m]	0.012	0.018	0.01	0.008
			e3p [m]	0.05	0.05	0.05	0.03
			pinchX [-]	0.5	0.1	0.1	0.1
			pinchY [-]	0.9	0.1	0.1	0.1
			damage1 [-]	0.01	0.019	0.019	0.02
			damage2 [-]	0.03	0.8	0.6	0.6
			Beta [-]	0.82	0.3	0.35	0.3
		Self-centering	k1 [N/m]	5.e6	5.e6	5.e6	5.e6
			k2 [N/m]	1.e3	2.e5	4.e4	9.e5
			sigAct [N]	22000	17000	16000	15000
			beta [-]	0.02	0.15	0.0	0.0
			epsSlip [-]	0.02	0.0159	0.015	0.011
			epsBear [-]	0.0	0.0	0.0	0.0
			rBear [-]	0.4	0.4	0.4	0.4

Table 21: Summary of the Input Parameters for the WE-Series and the Control Specimen

3.5.6. WG-Series

For modelling these shear dominated specimens, the pinching4 material was allocated to the shear spring. The flexure springs were assigned an elastic material. Subsequent to the plots of the outputs of the FE-model, the input parameters for all simulations of the WG-series are listed in the Table 22.

3.5.6.1. WG3

The hysteresis and the areas (Figure 106) match well for the specimen WG3. The backbone curves, shown in Figure 107, are equal until 5 mm. For larger displacements, they do not fit as well.

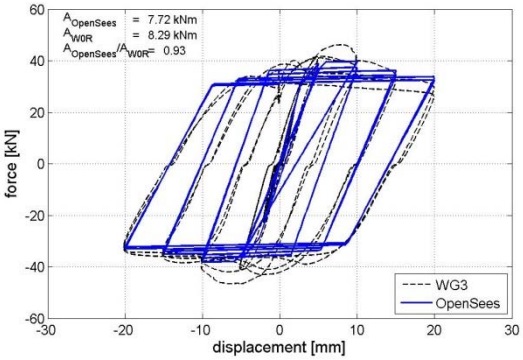

Figure 106: Comparison Hysteresis and Areas WG3

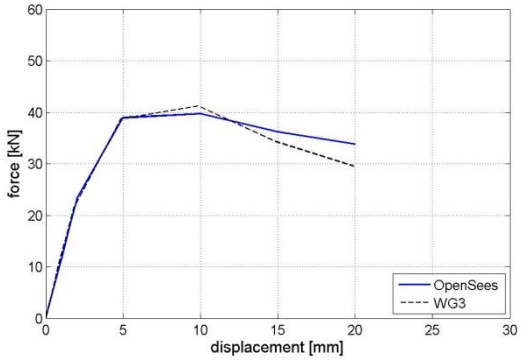

Figure 107: Comparison Backbone Curves WG3

For the first cycle's damping ratio, the values of the OpenSees model are consistently about 0.05 less than those from the experimental test of the WG3 specimen. The trend of the damping ratio of the second cycle comparison looks similar to the first cycle one. Only the value from the model with 15 mm amplitude is larger than the value from the experimental test.

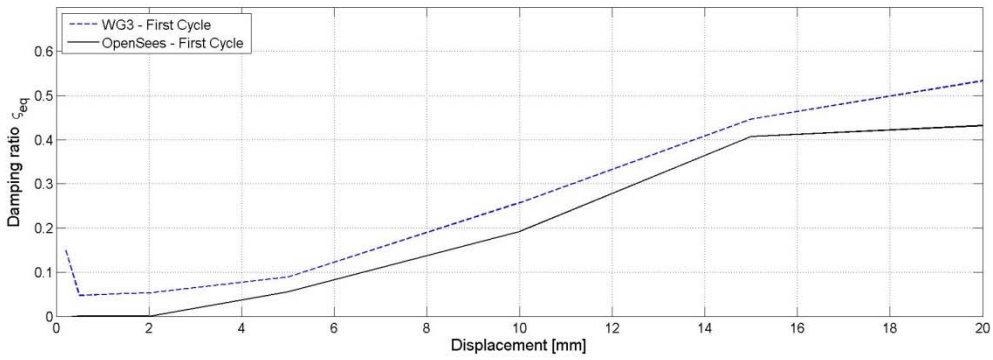

Figure 108: Comparison First Cycle's Damping Ratio WG3

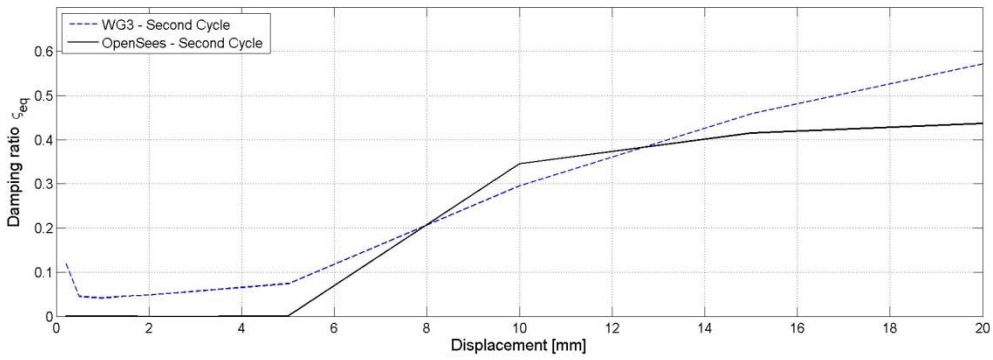

Figure 109: Comparison Second Cycle's Damping Ratio WG3

3.5.6.2. WG5

The output of the simulation is shown below with the hysteresis (Figure 110) on the left and the backbone curves (Figure 111) on the right. The backbone curve of the model is consistently below the experimental data for displacements larger than 5 mm.

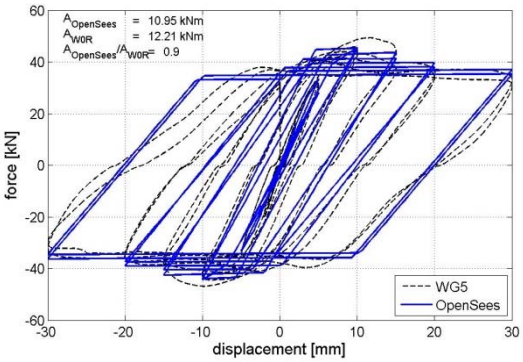

Figure 110: Comparison Hysteresis and Areas WG5

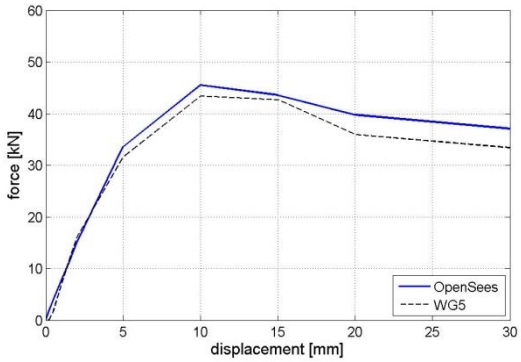

Figure 111: Comparison Backbone Curves WG5

Also the damping ratios for the first and the second cycle (Figure 112 and Figure 113) are less than the ones of the specimen WG5. By measuring small displacements (< 0.5 mm) the Potentiometers were not exact. Due to this fact, the peak in the experimental data's damping ratio was computed.

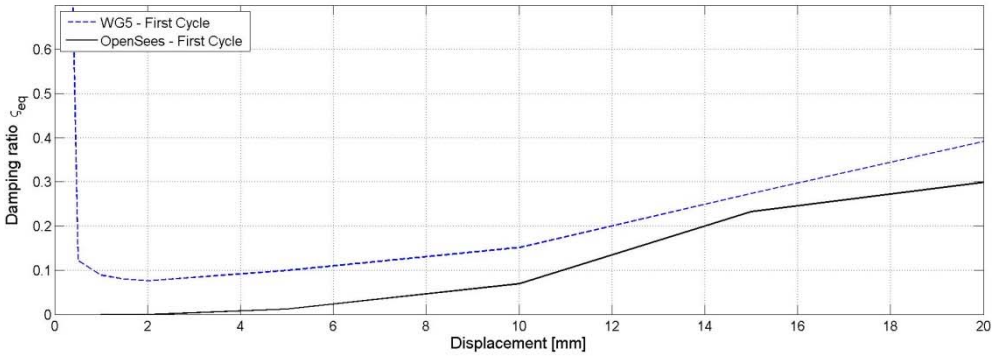

Figure 112: Comparison First Cycle's Damping Ratio WG5

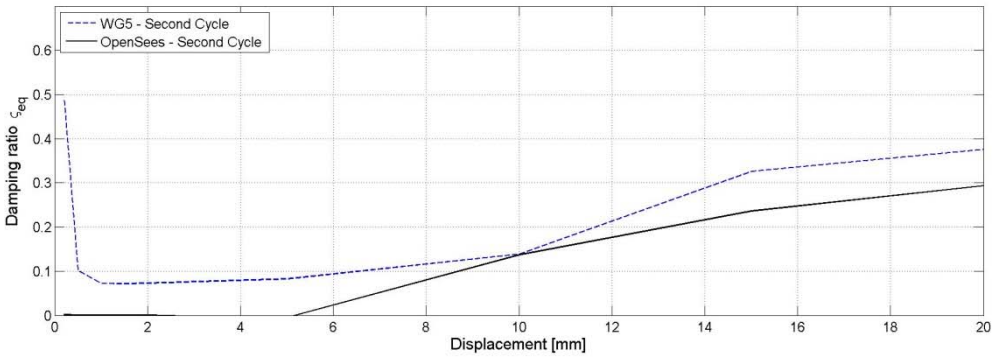

Figure 113: Comparison Second Cycle's Damping Ratio WG5

3.5.6.3. WG10

The comparison of the hysteresis is shown in Figure 114. The ratio of the areas is 0.89. In Figure 115 the backbone curves are compared.

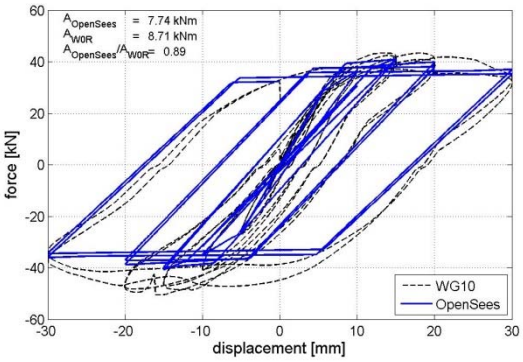

Figure 114: Comparison Hysteresis and Areas WG10

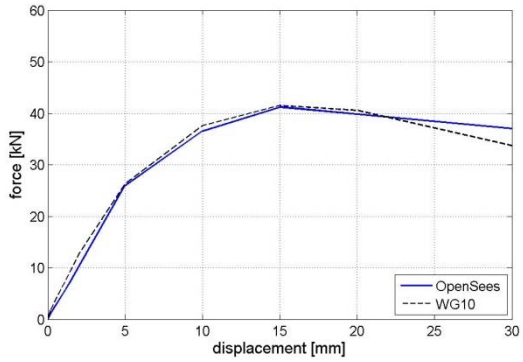

Figure 115: Comparison Backbone Curves WG10

The damping ratios (Figure 116 and Figure 117) of WG10 do not fit as well as they did for the other walls. For the second cycles, the simulation underestimates the energy dissipation significantly until the 10 mm amplitude cycle.

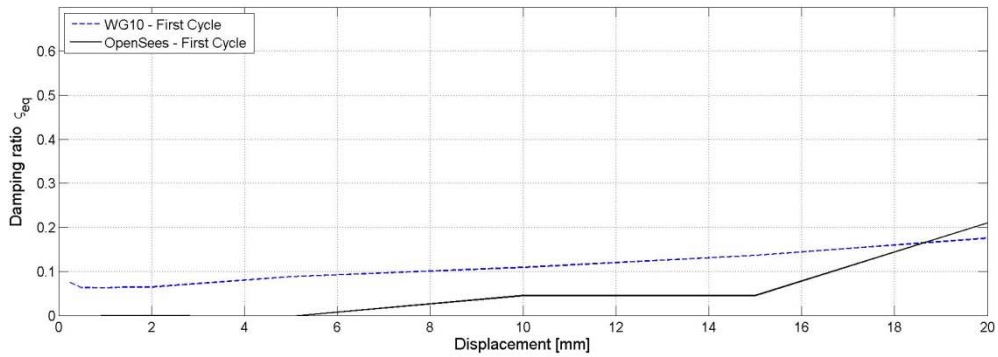

Figure 116: Comparison First Cycle's Damping Ratio WG10

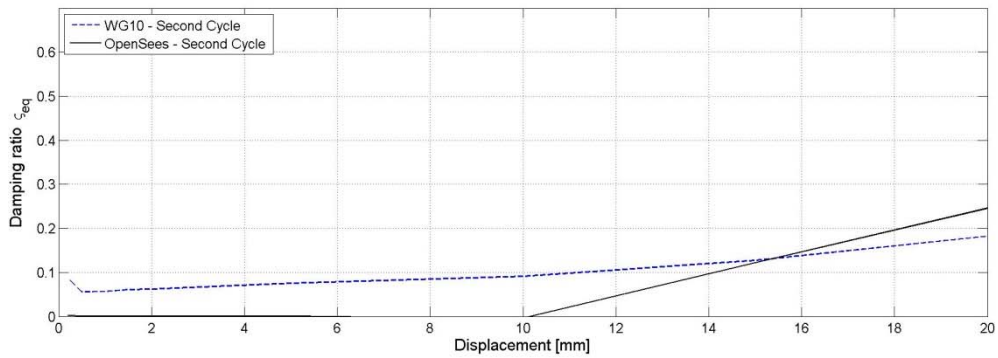

Figure 117: Comparison Second Cycle's Damping Ratio WG10

In Table 22 the input parameters of the OpenSees model for the WG-series are summarized.

Component	Material	Input parameter	WG3	WG5	WG10
Shear panel	Elastic	E [N/m]	4.1e7	4.1e7	4.1e7
Flexure spring	Elastic	E [N/m]	5e18	5e18	5e18
Shear spring	Pinching4	ePf1 [N]	33000	22000	28000
		ePf2 [N]	46000	40000	40000
		ePf3 [N]	47000	51000	47000
		ePf4 [N]	47500	52000	50000
		ePd1 [m]	0.002	0.002	0.004
		ePd2 [m]	0.005	0.005	0.01
		ePd3 [m]	0.02	0.01	0.015
		ePd4 [m]	0.04	0.035	0.035
		eNf1 [N]	-33000	-22000	-28000
		eNf2 [N]	-46000	-40000	-40000
		eNf3 [N]	-47000	-51000	-47000
		eNf4 [N]	-47500	-52000	-50000
		eNd1 [m]	-0.002	-0.002	-0.004
		eNd2 [m]	-0.005	-0.005	-0.01
		eNd3 [m]	-0.02	-0.01	-0.015
		eNd4 [m]	-0.04	-0.035	-0.035
		rDispP	1.0	1.0	1.0
		rForceP	1.0	1.0	1.0
		rDispN	1.0	1.0	1.0
		rForceN	1.0	1.0	1.0
		uForceP	0.95	0.98	0.95
		uForceN	0.95	0.98	0.95
		gK1	0.8	0.05	0.35
		gK2	0.2	0.8	0.25
		gK3	0.8	0.6	0.3
		gK4	0.2	0.2	0.05
		gKLim	0.8	0.65	0.8
		gD1	0.0	0.1	0.1
		gD2	0.0	0.5	0.2
		gD3	0.0	0.3	0.2
		gD4	0.0	0.05	0.1
		gDLim	0.0	0.4	0.4
		gF1	0.1	0.0	0.0
		gF2	0.3	0.4	0.4
		gF3	0.5	0.3	0.3
		gF4	0.2	0.3	0.3
		gFLim	0.8	0.5	0.5
		gE	10	10	10
		dmgType	“energy”	“energy”	“energy”

Table 22: Summary of the Input Parameters for the WG-Series

3.6. Conclusion of the Modelling Part

The BeamColumnJoint was chosen as the core element for the OpenSees model to efficiently simulate the behaviour of the specimens. With the BeamColumnJoint element, the model was simple to construct, but convergence problems occurred in the analysis, especially for the elastic-no tension material. To avoid the convergence failures, the input parameters of the material properties had to be chosen with careful consideration of the properties of the other components. By replacing the sensitive elastic-no tension material of the flexure springs with an elastic material, the model was no longer physically correct, but the simulations could be conducted in a more stable way. This course of action was needed to obtain satisfactory outputs.

Since the elastic-no tension material of the flexure springs was replaced with an elastic material, only the shear panel and the shear spring of the BeamColumnJoint element were used to simulate the observed test behaviour. The stiffness of masonry was allocated to the shear panel and left unaltered. The calibration of the model was done by adjusting the shear spring input properties only.

Before changing the model, the calibration was expected to be very difficult. Many input parameters had to be estimated to define the materials of the springs, though very little mechanical information about the soft-layers was known. Therefore the designated procedure was the trial-and-error method. This method was also used to select the shear spring properties after refining the model. However, the calibration was easier since only one component of the model (the shear spring) was to be calibrated.

The simulation of the different specimens worked well with the adapted model. Also the results fit quite well to the results of the experiments. The calibration of the model for all specimens was done by comparing the backbone curves, the shapes of the split hysteresis cycles, and the areas of the split hysteresis cycles. The damping ratios were not considered in the calibration phase. The FE-model damping ratios differed from the experimental damping ratios most significantly in the elastic range. The OpenSees simulation undergoes no energy dissipation during the displacement steps in the elastic range.

The quality of the calibrated model needs to be checked with future experiments. The model parameters were adapted for each specimen, so it is difficult to know whether the input parameters will represent the soft-layer's performance in a different test. This is especially true for the simulations of the specimens with rocking behaviour where the shear spring was forced to capture material and geometrical properties.

4. Overall Conclusion

The following observations can be made based on the tests conducted in this project:

1. The primary response mode of the control specimen W0R is rocking on the plane at the bottom of the wall. The maximum horizontal force capacity of the specimen (approximately 52 kN) is consistent with such mechanism. The magnitude of vertical load on the specimen is directly proportional to its horizontal force capacity. The control specimen sustained displacements of +/- 20 mm before failure.
2. The primary response mode of specimens WE3R, WE5R, and WE10 with the elastomer soft-layer bearings is rocking on the plane of the bearing (one brick layer above the bottom of the wall). Damage to the elastomer soft-layer wall bearing was slight (Figures 34-36). Maximum horizontal force capacity of the specimens (approximately 45 kN) is slightly less than that of the control specimen. No significant sliding was observed. The extent of the hysteresis loops suggests that specimens with the elastomer soft-layer wall bearing develop slightly more damping than the control specimen.
3. The primary response mode of specimens WG3, WG5, and WG10 with the granulate soft-layer bearing is a combination of sliding along the bearing and rocking on the plane of the bearing (one brick layer above the bottom of the wall). Damage to granulate soft-layer wall bearing was extensive (Figures 52-54). Maximum horizontal force capacity of the specimens (approximately 50 kN) is equal to that of the control specimen. The displacement capacity of the specimens with granulate soft-layer bearings is larger than that of the control specimen and depends on the thickness of the bearing. The thinnest bearing sustained slightly more displacement than the control specimen. The thickest bearing sustained approximately twice as much displacement as the control specimen without loss of horizontal force resistance. The extent of the hysteresis loops suggest that specimens with granulate soft-layer wall bearing develop significantly more damping than the control specimen or the specimens with elastomer soft-layer wall bearings.

Based on these obersvations we can conclude that the soft-layer wall bearing do not significantly reduce the horizontal force capacity of masonry walls. The magnitude of vertical load carried by the wall significantly affects its failure mode.

These results suggest that soft-layer bearings can be used to modify the seismic response of unreinforced masonry building structures. Additional experiments are required further understand the most appropriate material and thickness for the soft-layer. Another topic of future research is the investigation of the behaviour of the extruded elastomer soft-layers with rocking behaviour prevented. Material tests should be conducted with the different soft-layer materials. In addition to the dynamic mechanical analyses, which were conducted for both types of soft-layers, some tension and compression tests would be valuable.

Numerical modelling of the horizontal load-deformation response of unreinforced masonry walls with soft-layer bearings in OpenSees using the BeamColumnJoint element was reasonably successful. A number of different materials were investigated in order to find a combination that was not overly sensitive to convergence problems. The parameters of these materials were then calibrated to match the measured force-deformation response as well as possible. This calibration procedure was very difficult without more precise soft-layer and wall mechanical property data. Future work on the models sould investigate a more physically correct configuration of the shear panels, shear springs and the rocking springs to better represent the physical behaviour of the specimens.

References

American Society of Civil Engineers (ASCE), 2007. Seismic Rehabilitation of Existing Buildings (ASCE/SEI 41-06), Reston, VA.

Chopra, A. K. 2007. *Dynamics of Structures: Theory and Applications to Earthquake Engineering*. Prentice Hall, Upper Saddle River, NJ.

Griffith, M.C. & Page A.W. 1998. On the seismic capacity of typical DPC and slip joints in unreinforced masonry buildings. *Australian Journal of Structural Engineering*.

Mageba 2013. http://www.mageba.ch/

Menczel, J. D. & Prime, R. B. 2009. *Thermal Analysis of Polymer: Fundamentals and Applications.* John Wiley & Sons, Inc.,Hoboken, NJ

Lowes, L.N. & Mitra, N. 2004. A Beam-Column Joint Model for Simulating the Earthquake Response of Reinforced Concrete Frames, *PEER Report 2003/10*, University of California, Berkeley

Mojsilović, N. 2012. Masonry elements with damp-proof course membrane: Assessment of shear strength parameters. *Construction and Building Materials.*

Mojsilović, N., Simundic, G & Page, A. W. 2010. Masonry wallettes with damp-proof course membrane subjected to cyclic shear: An experimental study. *Construction and Building Materials*.

Mojsilović, N., Stojadinovic, B., Barandun, A. & Vögeli, C. 2013. Seismic behavior of masonry Walls with soft-layer wall bearings.

OpenSees, 2013. Open System for Earthquake Engineering Simulation. http://opensees.berkeley.edu/

Pacific Earthquake Engineering Research Center (PEER), 2013. http://peer.berkeley.edu/

Salmanpour, A., Mojsilović, N. & Schwartz, J. 2013. Experimental Study of the Deformation Capacity of Structural Masonry. 12th Canadian Masonry Symposium Vancouver, British Columbia

Simundic, G., Page, A.W. & Chen, Q. 2000. The cyclic and long term behaviour of slip joints in load-bearing masonry construction. *Proceedings of the 12th International Brick/Block Masonry Conference, Madrid.*

Swisscode SIA 266 Masonry Swiss Society of Engineers and Architects, Zurich, 2003

Zhuge, Y. & Mills, J. 1998. The behavior of masonry walls containing a damp proof course under cyclic loads. *Proceedings of the 2nd Australasian Structural Engineering Conference, Auckland.*

Appendix A: Rocking Force Level

The rocking force was computed with a simple model of a rigid body movement. A moment equilibrium was made about the location where B is at work. As soon as the equation is unequal, the body starts to move. The dimensions of the body (h and b) and the vertical force (V) remain fixed:

h = 1.15 m
b = 1.2 m
V = 100.9 kN

The drawing for the rotation about the edge of the body is shown in Figure 118 and the computation of the rocking force level for this composition below. The equation for the moment equilibrium is:

$$H \cdot h = V \cdot \frac{b}{2}$$

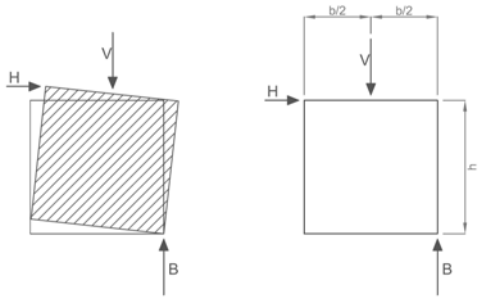

$$H = V \cdot \frac{b}{2h} = 52.7\ kN$$

Figure 118: Rigid Body with Center at the Edge

Figure119 shows the rigid body with the adapted center of rotation. The equation of the moment equilibrium has to be adapted to the geometry. The calculation was done analog.

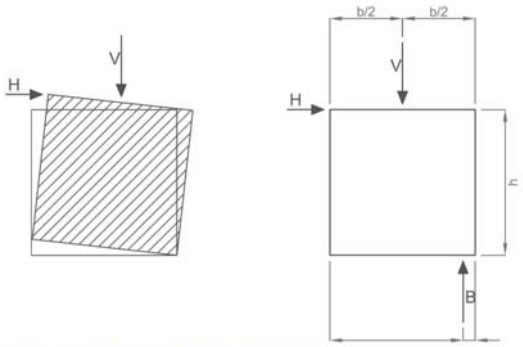

$$H = \frac{V}{h} \cdot \left(\frac{b}{2} - \frac{b}{12}\right) = 43.9\ kN$$

Figure 119: Rigid Body with Adapted Center

Appendix B: Digital Data

Below, the content of the compact disc is described.

1_administration:

- plagiarism_s_de.pdf
- ProjectOutline.pdf
- schedule.xlsx

2_Test setup:

- Autocad Inventor Teststand Brickwall: contains the files about the plan of the test setup
- Daten Werne: components of the library of the digital elements from the lab
- Measurement instruments: Figures of the measurement setup
- files of other parts of the test setup

3_calculations:

- roller_bearing: computations for defining the dimensions of the roller bearing
- deflection at reactionbeam.xlsx
- deflection of the masonry.xlsx: estimation of the elastic deflection of the masonry
- Force of the vertical jacks.xlsx: estimation of the vertical load equal to 10% of the strength
- versagen MW.pdf: expected failure of the masonry calculation

4_papers:

- Masonry: contains paper about masonry and similar test in the past
- Matlab: contains papers and documents which were used for creating some matlab scripts
- OpenSees: contains papers which explains parts from OpenSees
- Soft_layer: contains papers about polymers and DMA
- Structure_of_the_report: contains an example of a master thesis

5_pictures: contains the pictures taken during the work in the lab

6_Presentations:

- 1st_pres_Master_Thesis: contains the 1st presentation and pictures of it
- 2nd_pres_Master_Thesis: contains the 2nd presentation and pictures of it
- Final_presentation_Master_thesis: contains the final presentation and pictures of it
- Master_project_thesis: contains the presentation of the project thesis in fall 2012

7_data_of_the _tests:

- cleaned data: contains the cleaned data of the conducted tests
- whole_files: contain the whole files

8_Materials:

- bricks: contains the test results of the bricks

- mortat: contains the test results of the mortar prismns
- softlayer: contains the test results of the DMA of the Polymer Group

9_processing_and_simulation:

- **main_files**: contains the developed matlab and tcl files. The ones in here are the definitive versions. For running the matlab scripts it should be done in the correct order (start with the one with a_..., b_..., …) because in the output of the previous scripts sometimes is the input of the current script (example: before processing the data has to be loaded). Not all of the following scripts were used at the end, the imported ones are written bold. The matlab plots are also saved in this folder (saved by code).
    - **Data**: contains the output of the simulation with the OpenSees model. The output will be overwritten with each simulation.
    - loaded_data_24.05.13: contains structs for each specimen. The data is cleaned but not further processed. Meant as data backup.
    - **Matlab_plots**: contains plot of matlab for the technical report. The plots were saved by code to an appropriate size.
    - **a_load_DATA.m**: matlab script for loading, adapting, and saving the data. The data was saved in structs in matlab.
    - **AmirDATA**: matlab struct containing the horizontal force vector and the horizontal displacement vector of the test of Salmanpour et al. (2013), for estimating the material properties of the shear panel.
    - **b_datacheck.m**: matlab script to check the loaded data (visually)
    - **c_backbone_peak_disp_per_cycle.m**: matlab script for construction the backbone curve according to ASCE 41-06.
    - d_bbc_m.m: matlab script for construction the backbone curve of the masonry part of the specimen (NOT USED FINALLY)
    - e_bbc_SL.m: matlab script for construction the backbone curve of the soft-layer part of the specimen (over the joint containing the soft-layer) (NOT USED FINALLY)
    - **f_tot_area_env.m**: matlab script for containing the area in each cycle and also the whole area in the hysteresis
    - g_contribution_to_disp.m: matlab script from Dr. Catherine Whyte for computation the contribution of the displacements (NOT USED FINALLY)
    - h_disp_distribution_at_peaks.m: matlab file for calculation of the contribution of the displacements only at the cycle's peaks. (NOT USED FINALLY)
    - **i_damping_coefficient.m**: matlab script for calculation the damping ratio for all cycles
    - j_... – r_...: several matlab scripts for plotting
    - **LibGeneratePeaks_sine.tcl**: tcl script for creating the displacement time history which will be applied to the FEM-model.
    - **masonry.wall.withSL.tcl**: main tcl script. It defines the geometry, its elements and some of the materials (the rigid ones). Also the properties of the shear panel have to be changed in this script (it can be changed in line 84). It also conducts the the gravity analysis and defines the displacement amplitudes (line 298). It calls the other three required tcl scripts during the execution.
      With little changes, the material parameters of the springs below the shear panel can be inserted in this file (activate the line 164-224 and comment out line 227)
    - **OpenSees.exe**: OpenSees executor

- **OSDATA**: struct containing the data of the OpenSees simulation and furthermore processed data of it. The OS struct was overwritten after each simulation.
- **procsineRC.tcl**: tcl file for conduct the analysis of the horizontal load.
- Shear_Strain_Rect_and_Diagon.m: matlab script. This is a function of the g_contribution_to_disp.m. It is required for the calculation of the contribution.
- **SL_mat_par.tcl**: tcl file created with matlab. This file is called by the masonry.wall.withSL.tcl. It is used for defining the material parameter in matlab, thus the calibration was more effectively.
- **W0RDATA**: struct containing the data of W0R
- **WE3DATA**: struct containing the data of WE3
- **WE3RDATA**: struct containing the data of WE3R
- **WE5DATA**: struct containing the data of WE5
- **WE5RDATA**: struct containing the data of WE5R
- **WE10DATA**: struct containing the data of WE10
- **WG3DATA**: struct containing the data of WG3
- **WE5DATA**: struct containing the data of WE5
- **WG10DATA**: struct containing the data of WG10
- za_WG3_run_opensees_data.m: matlab script simulating the behaviour of specimen WG3. The input parameters of the OpenSees materials of the "soft-layer" springs are inserted in this file. By running this script, the FE-model will be run in OpenSees and the output data of the OpenSees simulation is loaded and processed (hysteresis plot and backbone curve plot). The calibration was made with rigid behaviour of the shear panel. Simulation with model with lack of physical correctness.
- **za_WG3_run_opensees_data_ShP.m**: analog za_WG3_run_opensees_data.m, but with the stiffness of the shear panel appropriate to the masonry (4.1e7 N/m)
- za_WG5_run_opensees_data.m: analog za_WG3_run_opensees_data.m.
- **za_WG5_run_opensees_data.ShP.m**: analog za_WG3_run_opensees_data.m, but with the stiffness of the shear panel appropriate to the masonry (4.1e7 N/m)
- za_WG10_run_opensees_data.m: analog za_WG3_run_opensees_data.m.
- **za_WG10_run_opensees_data.ShP.m**: analog za_WG3_run_opensees_data.m, but with the stiffness of the shear panel appropriate to the masonry (4.1e7 N/m)
- zb_WE3R_run_opensees_data.m: analog za_WG3_run_opensees_data.m.
- **zb_WE3R_run_opensees_data_ShP.m**: analog za_WG3_run_opensees_data.m, but with the stiffness of the shear panel appropriate to the masonry (4.1e7 N/m)
- zb_WE5R_run_opensees_data.m: analog za_WG3_run_opensees_data.m.
- **zb_WE5R_run_opensees_data_ShP.m**: analog za_WG3_run_opensees_data.m, but with the stiffness of the shear panel appropriate to the masonry (4.1e7 N/m)
- zb_WE10_run_opensees_data.m: analog za_WG3_run_opensees_data.m.
- **zb_WE10_run_opensees_data_ShP.m**: analog za_WG3_run_opensees_data.m, but with the stiffness of the shear panel appropriate to the masonry (4.1e7 N/m)
- zc_W0R_run_opensees_data.m: analog za_WG3_run_opensees_data.m.
- **zc_W0R_run_opensees_data_ShP.m**: analog za_WG3_run_opensees_data.m, but with the stiffness of the shear panel appropriate to the masonry (4.1e7 N/m)
- **zd_original_run_opensees_data.m**: analog za_WG3_run_opensees_data.m. But with the original (physically correct model)
- **zz__area_comp_OS_exp.m**: matlab script for comparing the cycle's shapes, computing the cycle's area, and the damping ratios of the OpenSees simulation.

    - **ZZZZZZZ_plots_for_report.m**: matlab script for plotting and saving the diagrams in an appropriate size.
- matlab_23.05.13: “old” matlab files. Finally not used
- OpenSees_23.05.13: OpenSees trials, examples, explanations, … Finally not used
- computation of the damage pinching4.xlsx: calculations of the damage of the pinching4 material. Finally it was not used.

10_technical report: contains the file of the technical report

11_drawings: contains the different drawings done with Autocad

12_poster: contains the poster

Appendix C: ETH Declaration of Originality

The declaration is on the next page.